https://doi.org/10.5194/egusphere-2025-3248
Preprint. Discussion started: 12 September 2025

Probabilistic and Deterministic Seismic Hazard Assessments of the area comprised between west Gulf of Cádiz and east Alboran Sea

Adrián José Rosario Beltré[1,2], Carlos Paredes Bartolomé[1], Miguel Llorente Isidro[3]

[1] Department of Geological and Mining Engineering, Higher Technical School of Mines and Energy, Universidad Politécnica de Madrid (UPM), Ríos Rosas 21, 28003 Madrid, Spain
[2] Department of Geological Resources for the Ecological Transition, Geological Survey of Spain (IGME), Spanish National Research Council (CSIC), La Calera 1, 28760 Tres Cantos (Madrid), Spain
[3] Department of Geological Risk and Climatic Change, Geological Survey of Spain (IGME), Spanish National Research Council (CSIC), Rios Rosas 23, 28003 Madrid, Spain

Correspondence to: Adrián José Rosario Beltré (aj.rosario@igme.es); Carlos Paredes Bartolomé (carlos.paredes@upm.es); Miguel Llorente Isidro (m.llorente@igme.es)

Abstract.

The increased deployment of subsea infrastructures and the exploration of marine resources have heightened the need to assess seismic hazard on the seabed, especially in tectonically active offshore regions. The area between the Gulf of Cádiz and the Alboran Sea, which is rich in coastal and submarine assets, is located within the Ibero-Maghrebian Region (IMR) a seismically active region. While previous research has addressed seismic hazard in adjacent inland areas using deterministic and probabilistic approaches, few studies have focused on offshore zones. Moreover, existing models often overlook the amplification effects introduced by bathymetry and seafloor conditions, and they rely on ground motion prediction equations (GMPEs) derived from inland data. Consequently, seismic hazard in marine environments remains poorly constrained. This study aims to evaluate the feasibility and applicability of both probabilistic (PSHA) and deterministic (DSHA) seismic hazard assessments for submarine areas, using updated seismogenic zonation, a high-resolution bathymetric model, and GMPEs suitable for soft marine soils. The objective is to produce reliable peak ground acceleration (PGA) estimates at the seabed and to examine the convergence of deterministic and probabilistic approaches in a complex tectonic context. The analysis was conducted using the OpenQuake (OQ) engine for PSHA and a custom MATLAB© script for DSHA. The seismogenic sources and parameters were taken from the ESHM20 model, and four GMPEs—IDR91, HZ23, NT24, and DKK24—were selected for their relevance to offshore or soft soil conditions. These GMPEs were validated against six regional offshore earthquakes recorded in the IMR. Hazard estimates were computed over a bathymetrically refined grid and expressed as PGA maps for various return periods (100, 475, 2475, and 5000 years). The results show that significant PGA values occur over key submarine fault systems such as the Gorringe Ridge, Horseshoe Plain, and Arzew Fault. Offshore PGA estimates for return periods of 2475 years using NT24 and DKK24 are close to those derived from DSHA, settling convergence between methodologies. The use of seabed-adapted GMPEs resulted in higher and more realistic PGA values compared to inland

https://doi.org/10.5194/egusphere-2025-3248
Preprint. Discussion started: 12 September 2025

models. This study demonstrates the applicability of seismic hazard assessment methods to offshore environments and highlights the importance of incorporating seafloor conditions into hazard modelling. The findings offer a methodological basis for improving the seismic design of subsea infrastructure in tectonically complex marine regions such as the IMR.

1. Introduction

The majority of ocean infrastructures are anchored or seated on the seabed in some way (e.g., Guo et al., 2021; Rui et al., 2024). The stability of these assets may be compromised by the mechanical properties of the seafloor (e.g., Liu et al., 2021; Randolph and Gourvenec, 2017; Veiskarami et al., 2017). Earthquakes and the processes they trigger, such as tsunamis and landslides, affect the dynamic behaviour of the ground, with the potential to cause significant damage to infrastructures and facilities (Román-de la Sancha et al., 2022; Shan et al., 2022). Consequently, attention should be given to investigate local effects on offshore structures (e.g., Kee et al., 2023; Li et al., 2023) along with undersea seismic hazard and the influence of surrounding seismogenic sources (Ercilla et al., 2021; Karthigeyan, 2022). Coastal and offshore facilities should be designed to withstand earthquakes and their coseismic effects. Research show that the seawater layer and seafloor cohesion mainly influence how seismic energy is transmitted in marine environemnts (Chen et al., 2024; Lan et al., 2021). However, the strategies to evaluate undersea seismic hazard may not be entirely valid considering they rely on seismic response of emerged terrain.

The area encompassing the Strait of Gibraltar, between the Alboran Sea in the Mediterranean Sea and the Gulf of Cádiz in the Atlantic Ocean, is also known as the Ibero-Maghrebian Region (IMR) (Buforn et al., 1995). A substantial number of communication and energy cables (Submarine Cable Map, 2025) are present in the IMR. Major infrastructures are also located here, including oil and gas pipelines connecting Algeria and Morocco with Spain (Medgaz; https://www.medgaz.com/, last accessed 08/07/2025) and several offshore wind farms. Moreover, the European-African tunnel is planned to be developed in the IMR (SECEGSA; https://www.secegsa.gob.es/proyecto-del-enlace-fijo, last accessed 08/07/2025). These assets, among other issues, underscore the area's substantial geostrategic importance (Báez et al., 2021). The IMR is at the boundary between the Eurasian and Nubian tectonic plates (Buforn et al., 2016). It comprises the southern Iberian Peninsula and the Maghreb (Buforn et al., 1995), and it is considered to have a medium to moderate tectonic activity, with frequent seismicity due to the convergence of the tectonic plates. Significant and devastating earthquakes have been documented within the region (Buforn et al., 2015), some of which have triggered tsunamis and submarine landslides (Table 1). Consequently, a comprehensive Seismic Hazard Assessment (SHA) is of utmost relevance within the IMR.

Nowadays, there are two broad standard approaches to Seismic Hazard Assessment (SHA, Hamidatou et al., 2024; Kumar et al., 2024): Deterministic Seismic Hazard Analysis (DSHA) and Probabilistic Seismic Hazard Analysis (PSHA; Reiter, 1990). These methods have also been criticised (Kossobokov and Panza, 2022). Currently, PSHA has been broadly adopted by the scientific community and for mitigation plans, whilst DSHA is still considered useful in worst-case scenario modelling

https://doi.org/10.5194/egusphere-2025-3248
Preprint. Discussion started: 12 September 2025

situations (Grasso and Maugeri, 2012; Mostafa et al., 2019), commonly used by civil protection agencies. DSHA was the first methodology proposed in the late 1960s for the design of nuclear power plants and was later applied to other large industrial infrastructures (AEIS-IGN, 1979; NRC, 1973). DSHA and PSHA can complement each other, providing further information about the existing seismic hazard (Wang et al., 2012).

Table 1: Location, date and moment magnitude (M_w) of some large earthquakes with causalities in the IMR.

Region	Location	Date	M_w	Casualties	Reference
Southern Iberian Peninsula	Malaga, Spain	10.09.1680	6.8	70	Goded et al. (2008)
	Lisbon, Portugal	11.01.1755	7.7	100,000	Chester (2001), Fonseca (2020)
	Torrevieja, Alicante	03.21.1829	6.8 - 6.9	389	Silva et al. (2019)
	Andalusian, Spain	12.25.1884	6.5 - 6.7	839	Udias and Muñoz (1979)
	Adra, Almeria	06.16.1910	6.1	0	Stich et al. (2003)
	Cape St. Vincent, Portugal	02.28.1969	7.8	19	López Arroyo and Udías (1972)
North Africa	Oran, Algeria	09.10.1790	6.0 - 6.5	2,000	Ayadi and Bezzeghoud (2014)
	El-Asnam, Algeria	10.10.1980	7.3	2,633	Ayadi and Bezzeghoud (2014)
	Boumerdès, Algeria	05.21.2003	6.8	2,278	Ayadi and Bezzeghoud (2014)
	Al-Hoceima, Morocco	02.24.2004	6.3	629	Kariche et al. (2018)

Despite the significant record of earthquakes, submarine landslides and tsunamis in the IMR (Rodriguez et al., 2017; Vázquez et al., 2022), the area has not been updated in full SHA. The first attempt of SHA in IMR was made by Molina Palacios (1998). This work evaluates the seismic hazard in terms of intensities and PGAs of the Iberia-Africa contact zone by a probabilistic approach. This involved a seismic zonation using areal sources, applying available estimation tools to flat terrain, using ground motion prediction equations (GMPEs) from rocky inland areas, and relying on seismotectonic knowledge from the 1990s. Conversely, the emerged land around the IMR has exhaustive seismic hazard studies, using both deterministic and probabilistic approaches. For example, the PHSA method has been the most widely implemented (e.g., Crespo et al., 2014; Danciu et al., 2024; IGN-UPM, 2017; Salgado Gálvez et al., 2015). Neo-deterministic Seismic Hazard Assessment (NDSHA) has been applied for the Iberian Peninsula (García-Fernández et al., 2022) and DSHA for Sevilla city (Sá et al., 2021). In the North African part, Poggi et al. (2020) performed a PSHA, and Mourabit et al. (2014) also conducted an NDSHA approach in this region. At the European continental scale, the most recent work covers the Euro-Mediterranean region, where the IMR is located. A fully probabilistic framework was adopted in the implementation of the hazard model, using harmonised input datasets across national boundaries. The seismogenic zone mosaic uses the 2020 European Seismic Hazards Model (ESHM20) (Danciu et al., 2024) for PSHA hazard assessment. The ESHM20 model uses the same principles as the 2013 Seismic Hazard Harmonisation in Europe (SHARE) project model (ESHM13) (Wössner et al., 2015), with state-of-the-art procedures applied homogeneously to the pan-European region. However, the SHA gap in the marine environment persists, hence further assessment of large-scale seismic hazard under seabed conditions within the marine IMR is needed, taking into consideration

https://doi.org/10.5194/egusphere-2025-3248
Preprint. Discussion started: 12 September 2025

earthquake characteristics and spatial distribution based on comprehensive undersea data. In order fill this gap, this study has used seismic zoning and parameters from the ESHM20 (Danciu et al., 2021a, 2024). The novelty of this work also involves the use of attenuation functions derived from analogous marine regions regarding their seismotectonic context, considering there are no estimates of GMPEs for the IMR at this time. The DSHA here has been carried out using an in-house development, while for the PSHA the OpenQuake engine software was used (OQ v3.21) (Pagani et al., 2014; Silva et al., 2014).

2. Study area

The study area is characterized by a complex geodynamic context resulting from the interaction between the Nubia and the Iberian tectonic plates (Fig. 1) (e.g., Custódio et al., 2016; Neres et al., 2016). The plate boundary of the study area is usually divided into three main areas according to their stress regime: the SW as simple shear zone, the pure shear Gulf of Cádiz as the Eastern Betic, and the South Moroccan compressional arc. Tectonic models of NW-SE to WNW-ESE show oblique convergence between the Nubia and Iberian plates (Herraiz et al., 2000; Reilly et al., 1992) with displacements of 2 to 5 mm/yr (Fernandes et al., 2007; Nocquet, 2012) of the western Betic Cordilleras with respect to the Iberian Massif (Gonzalez-Castillo et al., 2015; Palano et al., 2013).

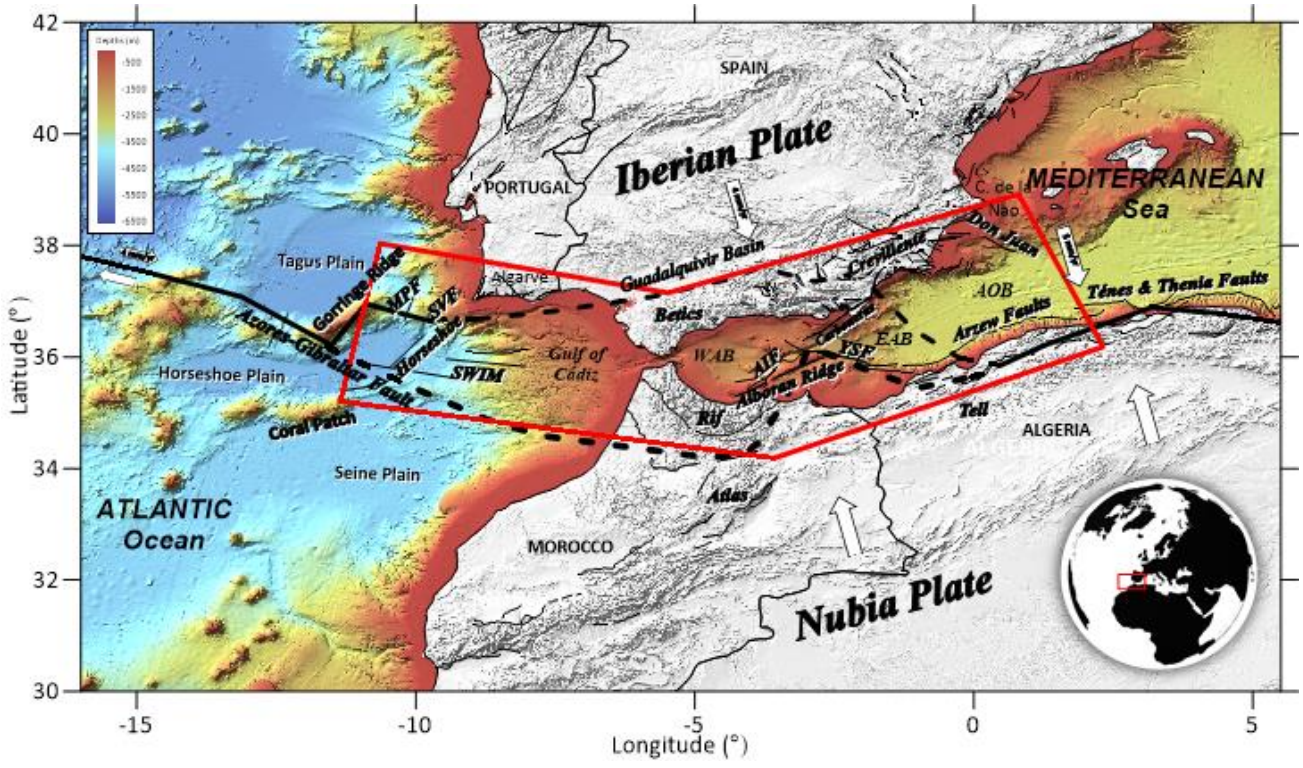

Figure 1. Location of the area of interest of this work in relation to the tectonic setting. Abbreviations are as follows: WAB: Western Alboran Basin, EAB: Eastern Alboran Basin, AOB: Algerian Oceanic Basin, SVF: Sao Vicente Fault, MPF: Marques de Pombal fault, SWIM: Southwest Iberian Margin lineaments (1, 2 and 3). AIF: Al Idrisi fault, YSF: Yusuf fault. Background: shadowed

https://doi.org/10.5194/egusphere-2025-3248
Preprint. Discussion started: 12 September 2025

Digital Terrain Model (altimetry and coloured bathymetry) in the study area (extracted from EMODnet; https://emodnet.ec.europa.eu/en/bathymetry).

The Gulf of Cádiz (western sector of IMR) is located on the contact boundary between the Eurasian and African plates. It extends from the Azores Islands to the Strait of Gibraltar, through the Iberian massif and the Algarve region to the north, and, in the eastern part, through the orogenic arc of the Betic-Rifeña mountain range. It is characterised by a NW-SE oblique convergence regime, mainly controlled by the formation of the Betic-Rifeño Orogen and by the accommodation of post-orogenic compressional tectonic activity (IGN, 2025a). This tectonic configuration makes seismic activity in the Gulf of Cádiz significant, with moderately deep earthquakes (h < 40 - 60 km) (Custódio et al., 2016). Some moderate magnitude earthquakes have also been recorded (Martín-Dávila and Pazos, 2003). Most of the focal mechanisms in this area are reverse and rifting type. There is also historical and instrumental evidence of several high-magnitude earthquakes in the region. These include the earthquakes of 1755 (M_w 7.7; Chester, 2001; Fonseca, 2020) and 1969 (M_w 7.8; López Arroyo and Udías, 1972), both causing tsunamis that affected the coasts of Morocco, Portugal, and Spain. The Gorringe Bank, the Sao Vicente submarine canyon (Sao Vicente fault), Horseshoe, Marqués de Pombal, and the Southwest Iberian Margin (SWIM) faults show the greatest magnitudes in the region (M_w 7.2 – 8.4; Grevemeyer et al., 2017; Martínez-Loriente et al., 2013) surrounded by the Gorringe Ridge, the Coral Patch, the Horseshoe and Seine abyssal plains.

The Alboran Sea is the westernmost part of the Mediterranean Sea and the oriental sector of IMR. It is bordered by the Alpine Mountain ranges of the Betic in the Iberian Peninsula and the Rif in the north of Africa. It is a complex contact zone between the converging Eurasia and Nubia tectonic plates. Among the tectonic structures, the submarine mountain ranges stand out, with a length of more than 50 km, oriented NE-SW and limited to the north and south by reverse faults with opposite dip. Several sets of conjugate directional faults are also found in this area: the NNE-SSW sinistral faults, such as the Al-Idrisi; the NE-SW sinistral faults, such as the Carboneras; and NW-ESE dextral faults, such as the Yusuf. Most of the seismic events recorded in the Alboran Sea have lower magnitudes (M_w < 4 , IGN, 2025b). The seismic activity in the Alboran Sea is interconnected with the southern Iberian Peninsula through the tectonic system running E-W from the Rif and Alboran Ridge, Eastern Alboran Basin, to the Arzew faults and Tell Atlas (e.g., Mourabit et al., 2014; Leprêtre et al., 2018). Some relevant events in the Alboran Sea are the Adra earthquake in 1910 (M_w 6.1; Stich et al., 2003), and the Al Hoceima earthquakes of 1994 (M_w 6.0), 2004 (M_w 6.3) and 2016 (M_w 6.4) (Kariche et al., 2018).

Most recorded earthquakes in the IMR are between 0 and 30 km, although a considerable number of earthquakes are of intermediate depth ($30 \leq h \leq 180$ km), mostly located in the Gulf of Cádiz (IGN, 2025c). Deeper earthquakes ($h \geq 600$ km) are less frequent and located in the province of Granada (Buforn and Udías, 2007). About 90% of the registered seismicity in the IMR is located in the Gorringe Bank, High Atlas and the Granada-Malaga-W of Alboran Sea area. In the Alboran Sea, there is also significant shallow seismicity at depths of less than 30 km, especially in the active Betico-Alboran-Rif shear zone; to the W, earthquakes go deeper.

https://doi.org/10.5194/egusphere-2025-3248
Preprint. Discussion started: 12 September 2025

3. Materials

For seismic hazard estimation on the seabed, using the DSHA and PSHA methods, the following input parameters are required: a) a digital terrain model (DTM); b) seismogenic sources and their associated seismic parameters; and c) GMPEs.

3.1 Ocean and land digital terrain models

The DTM used in this study was obtained from the EMODnet Bathymetry World Base Layer (EBWBL), composed of the bathymetric grid for Europe from the European Marine Observation and Data Network (EMODnet; https://emodnet.ec.europa.eu/en/bathymetry) (Martín Míguez et al., 2019), with spatial resolution of 4 arc seconds, and the raster for oceans and land from the General Bathymetric Chart of the Oceans (GEBCO; https://www.gebco.net/) (GEBCO Bathymetric Compilation Group 2024, 2024; Mayer et al., 2018), with a spatial resolution of 15 arc seconds.

3.2 Seismogenic Source Models and Seismicity Parameters

Considering the SHAs carried out in the emerged IMR zone, several seismogenic source models have been identified (Fig.1, Table 2). The one implemented in the ESHM20 (Danciu et al., 2021a, 2024) has been used for this work given it is the latest update. This zonation includes areal seismogenic sources (shallow and deep), active faults and background smoothed seismicity (Fig. 2). To achieve our SHA, all seismic sources influencing our study area were incorporated, together with their corresponding characteristic seismic parameters.

Table 2: Some seismogenic zonation models covering the study area.

Zonation model	Covered extension	Reference	Implementation
SA and SB	Portugal	Vilanova and Fonseca (2007)	Seismic hazard map of Portugal
ZESIS or COMMISSION	Iberian Peninsula	García Mayordomo (2015)	Seismic hazard map of Spain
NAF	North Africa	Poggi et al. (2020)	Seismic hazard map of North Africa
SHARE- ESHM13	Euro-Mediterranean region	Wössner et al. (2015)	Seismic hazard map for Europe
ESHM20	Euro-Mediterranean region	Danciu et al. (2024)	Seismic hazard map for Europe

The seismic parameters used for the DSHA (Fig. 2), were extracted from the ESHM20 model (Danciu et al., 2021a, b). The maximum magnitude $<MM_{max}>$ from the maximum magnitude distribution function, was adopted as the maximum credible earthquake (MCE) along with the predominant rupture mechanism assigned to each planar source ID at its depth (Tables S1 and S2 in supplementary material). The areal seismogenic sources are located at depths ranging from 12 to 60 km (Fig. 2 A1). Seismic features derived from Active Shallow Crustal Region (ASCR) seismogenic sources have magnitudes ranging from 6.6 to 8.8 (Fig. 2 A3). The predominant rupture mechanism is inverse in the band from the Gulf of Cádiz towards the Algerian Mediterranean coast, through the southern Rif and parallel to the Atlas chain (Fig. 2 A2, B2 and C2). This rupture mechanism transitions into strike-slip toward the Alboran Sea and the adjacent Iberian coastal zone, while evolving into normal

https://doi.org/10.5194/egusphere-2025-3248
Preprint. Discussion started: 12 September 2025

faulting further inland within the Iberian Peninsula. The deep source beneath the Strait of Gibraltar (~150 km) was initially discarded in line with the original DSHA approach, since it is outperformed by shallower ASCR sources. However, this work includes the distribution of all seismic sources even if their attenuation make them negligible at any given point. The active faults are located at depths ranging from 6 to 25 km (Fig. 2 B1) and magnitudes ranging from 6.9 to 8.5 (Fig. 2 B3). For the background smoothed seismicity, point sources have depths ranging from 12 to 60 km (Fig. 2 C1) and magnitudes ranging from 6.5 to 8.6 (Fig. 2 C3). For the PSHA, the same dataset used in the ESHM20 model has been used Danciu et al. (2021b, c). These files include all the seismogenic sources and their characteristic parameters, required to carry out the probabilistic calculation in our study area. Since we adopted the same calculation software (OQ Engine) used in the ESHM20 model for the seismic hazard calculation, it was not necessary to modify the seismogenic source files.

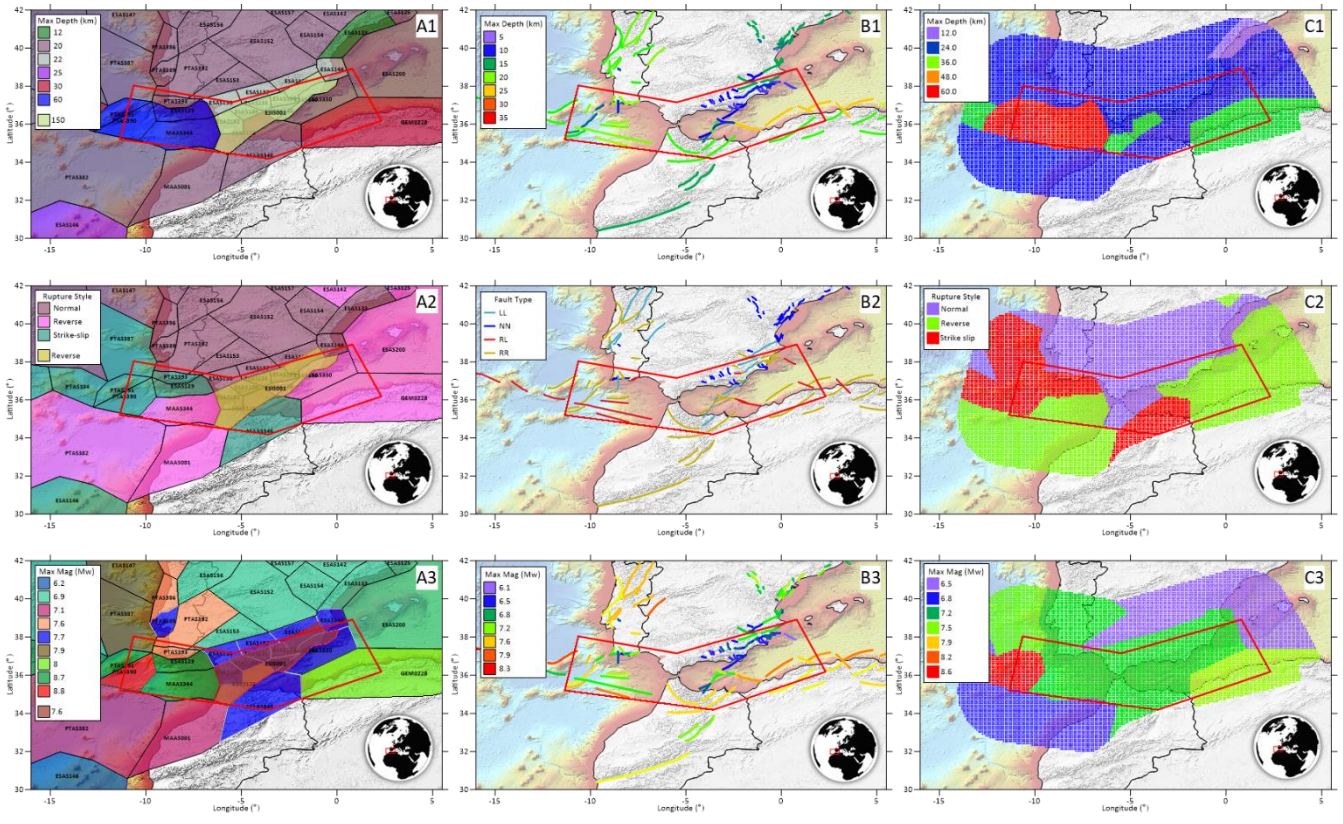

Figure 2. Seismogenic source models of ESHM20: (a) areal seismogenic sources (shallow and deep); (b) active faults and (c) smoothed seismicity; in function of (1) Depth (km), (2) Predominant rupture mechanism for each seismogenic source, and (3) Magnitude of maximum credible earthquake (MCE). (Data from Basili et al., 2024; Danciu et al., 2021b, 2024).

https://doi.org/10.5194/egusphere-2025-3248
Preprint. Discussion started: 12 September 2025

3.3 Ground motion prediction equations (GMPEs)

GMPEs are essential in seismic hazard analysis, as they model how ground motion attenuates with distance. These equations estimate shaking intensity at a site based on factors like earthquake magnitude, distance to the source, faulting style, and local geological conditions (Barani et al., 2016). GMPEs are commonly derived from strong ground-motion records for an earthquake (e.g., Campbell and Bozorgnia, 2003). Functions relate the magnitude M and the distance R of the seismic scenario (M, R). With an appropriate set of quality records, it is possible to fit a parametric model $f(M,R,\phi_k)$ to estimate the intensity of strong motion (Y) for a given seismic scenario. The fitted parameters reflect the characteristics of elastic and anelastic energy attenuation through distance scaling, but also near and far-source, faulting mechanism, and hanging wall effects. The heterogeneous geological media causes a dispersion in the (M, R) sample pairs. Therefore, the correlation between variables can be strong, but never perfect, meaning there is an unavoidable uncertainty ε. If the expected seismic intensity at the project site Y is interpreted as a conditional random variable on the pair (M, R), the fitted model (Atik et al., 2010):

$$Y \sim f(M,R,\phi_k) + \varepsilon \quad (1)$$

provide an estimate of the median ground motion and the residual ε (Akkar et al., 2013) identified by a Gaussian distributed random variable.

Most GMPEs are defined in terms of relative fault distance to the SHA site assuming a planar rupture geometry. The rupture trace is defined as the projection of the upper edge of the rupture onto the ground surface. The rupture plane, trace, and surface projection allow the definition of four finite fault distance metrics: R_{RUP}, R_{JB}, R_X, R_Y, Z_{TOR} (Fig. 3). R_{RUP} is the closest distance between the site and the rupture surface. R_{JB} is the Joyner and Boore distance or the closest distance between the site and the surface projection of the rupture. R_X is the horizontal and R_Y the vertical distance between the site and the top edge of the rupture. Finally, Z_{TOR} is the depth to the top edge of the rupture. These metrics are commonly incorporated in GMPEs, as R in in the mathematical formulation of Eq. (1) (e.g., Douglas, 2020). Some of the GMPEs formulation Eq. (1) consider the distance R as a function of depth (e.g., R_{RUP}). In these cases, the estimation of the intensity of the motion is affected by the terrain relief where the site is located. Thus, the estimated shake motion Y in elevated areas will be lower than in marine abyssal plains because they are closer to seismogenic sources, and the results of Y estimation in regions with significant unevenness will be sensitive to the use of a DTM.

The wealth of available strong ground motion data has enabled the development of numerous GMPEs, the vast majority on the rocky ground inland (e.g., Douglas, 2020). However, in offshore regions, traditional rock-based models may not adequately capture the unique conditions of the sea floor (Chen et al., 2024; Tan and Hu, 2023; Wang et al., 2024). The growing importance of subsea structures and the associated risks of seabed instability have prompted the development of efforts to obtain GMPEs for offshore areas. Nevertheless, the limited availability of data and the scarcity of strong motion records have restricted their collection to very few offshore areas. A significant proportion of recent research has focused on the active area

https://doi.org/10.5194/egusphere-2025-3248
Preprint. Discussion started: 12 September 2025

of the Japan Trench using the S-net and KiK-net stations data (Kanazawa et al., 2016), where several GMPEs have been recently developed (e.g., Dhakal et al., 2024; Hu et al., 2020, 2023; Nakanishi and Takemura, 2024).

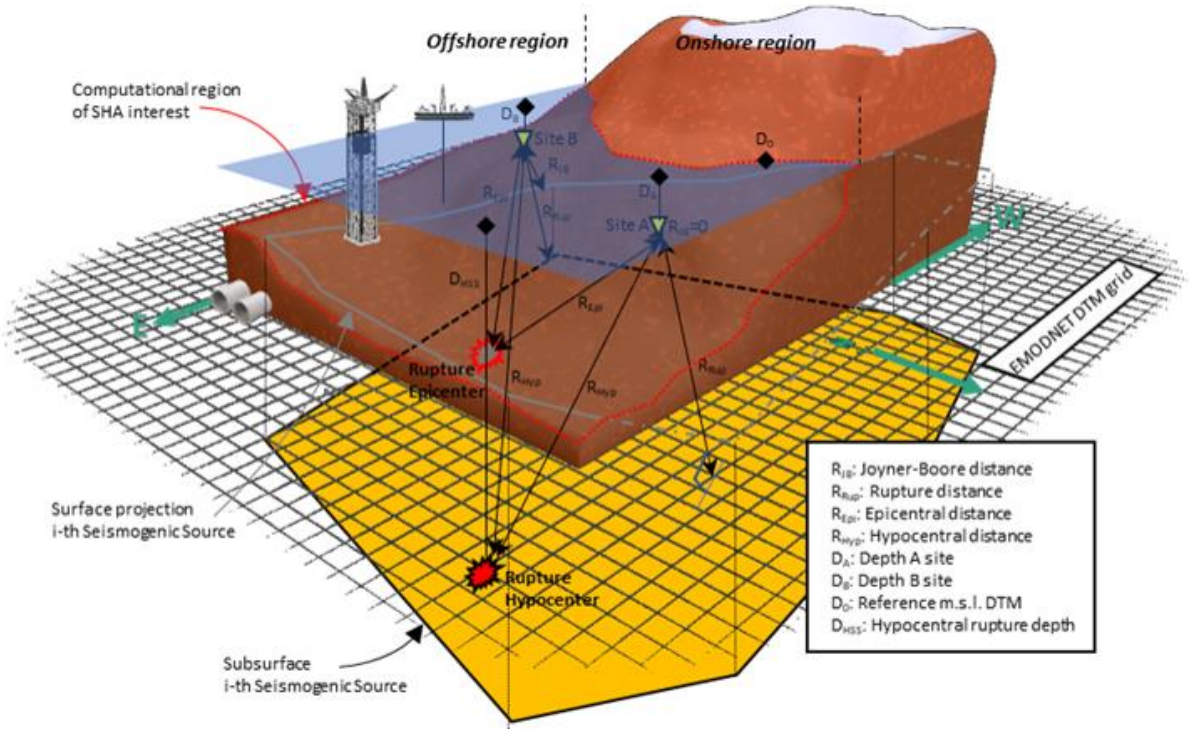

Figure 3. Earthquake source and distance metrics from an offshore evaluation site in and out a seismogenic source area. Site A outside the ground projection of the seismogenic source, with (H≠0) and without surface altimetry or bathymetry (H=0). Site B inside the ground projection of the seismogenic source, without surface altimetry or bathymetry (H=0).

For soft soils, a GMPE model was already described by Idriss (1991) in the early 1990s (IDR91). The IDR91 model is suggested for the entire moment magnitude range and a distance of 0-100 km or more. The Joyner-Boore metric is used as the source-to-site distance (R_{JB}) to obtain Ln (Y), where Y is in g, and the uncertainty (ε) in Ln (Y) depends on the earthquake magnitude in the function described by Idriss (1991) if $M_w < 7.25$, otherwise the standard error term is constant (ε = 0.38). This model is suited for crustal earthquakes and it has been implemented in SHA for submarine zones in the Mediterranean Sea (e.g., D'Acremont et al., 2022; Lafuerza et al., 2012; Sultan et al., 2007). Therefore, IDR91 was also considered in this work to compare it with other recent approaches to offshore GMPEs. Recently, the HZ23 model (Hu et al., 2023), has been developed for offshore earthquakes in the Japan Trench area and derived from onshore model ZH06 (Zhao et al., 2006). HZ23 was developed for M_w between 4.0 and 7.1, and hypocentral distances of 20-300 km. This model uses R_{RUP} as distance metric in Eq. (1) for crustal, interface, and slab events to obtain Ln (Y) with a constant standard error (ε = 0.7784), where Y is in

https://doi.org/10.5194/egusphere-2025-3248
Preprint. Discussion started: 12 September 2025

cm/s². Additionally, the averaged shear-wave velocity to 30 m depth (Vs30) was incorporated as a parameter in Eq. (1) for the definition of the site class. The NT24 model (Nakanishi and Takemura, 2024), was also developed for the Japan Trench area and derived from the onshore model MF13 (Morikawa and Fujiwara, 2013). It can assess PGAs for M_w between 5.5 and 7.4 for crustal, intraplate, and slab earthquakes (M_w > 5.0 for crustal events) and epicenter distances of 1 to 300 km. This model uses R_{RUP} to obtain $\log_{10}$ (Y) with a constant standard error (ε = 0.326). Finally, the DKK24 model (Dhakal et al., 2024) was developed for M_w between 5.5 and 7.4, and hypocentral distances of 1 to 300 km. This model uses R_{RUP} as distance metric in Eq. (1) for crustal, interplate and intraslab events to obtain $\log_{10}$ (Y) with a constant standard error (ε = 0.25183). Therefore, four GMPEs have been used in this work —IDR91, HZ23, NT24, and DKK24— (Fig. 4), considering both the seminal studies on soft soils and recent work proposing new GMPEs for submarine environments. In this study, the PGA (g) is the Y seismic intensity used in all of these selected attenuation functions. A unit weighting was assigned to each GMPE for the SHAs.

The predominantly offshore setting of the study area —at the intersection of oceanic, active continental, and stable continental crust— poses significant challenges for selecting appropriate GMPs. Recent tectonic classifications (Chen et al., 2018; Poggi et al., 2020) describe the study region as a Variscan-Hercynian zone in an Active Shallow Crustal Region (ASCR). In the case of the HZ23, NT24 and DKK24 models and their implementation in our study area, the IMR and the Japan Trench area share some geo-tectonical similarities. In the IMR, the African Plate is subducting beneath the Eurasian Plate (Gutscher et al., 2002), while in the Japan Trench area, the Pacific Plate is subducting beneath the Okhotsk Plate (Nishikawa et al., 2023). Both areas experience significant seismic activity due to the tectonic interactions. The IMR has a history of large earthquakes (Buforn et al., 2015), while the Japan Trench area is known for its frequent and intense earthquakes, including the devastating 2011 Tōhoku earthquake (Ritsema et al., 2012).

In addition, the performance of the GMPEs was evaluated against observed ground motions from six offshore earthquakes in the IMR (Fig. 4) including five crustal and one intraslab event. A comparative analysis of IDR91, HZ23, NT24, and DKK24 was conducted using the following events:

1) M_w 4.5 Alboran Sea earthquake, 31/01/2016 (Fig. 4A),
2) M_w 4.9 Alboran Sea earthquake, 04/01/1994 (Fig. 4B),
3) M_w 5.5 Oran earthquake, 06/02/008 (Benfedda et al., 2020) (Fig. 4C),
4) M_w 6.1 SW Cape St. Vincent earthquake, 12/02/2007 (Fig. 4D)
5) M_w 6.3 Alboran Sea strike-slip earthquake, 25/01/2016 (Fig. 4E),
6) M_w 6.8 Boumerdès Earthquakes, 21/05/2003 (Khellafi et al., 2013) (Fig. 4F).

The acceleration data for earthquakes in Fig.4 (A), (B), (D), and (E) are sourced from IGN (https://www.ign.es/web/sis-catalogo-acelerogramas, last accessed 08/07/2025).

https://doi.org/10.5194/egusphere-2025-3248
Preprint. Discussion started: 12 September 2025

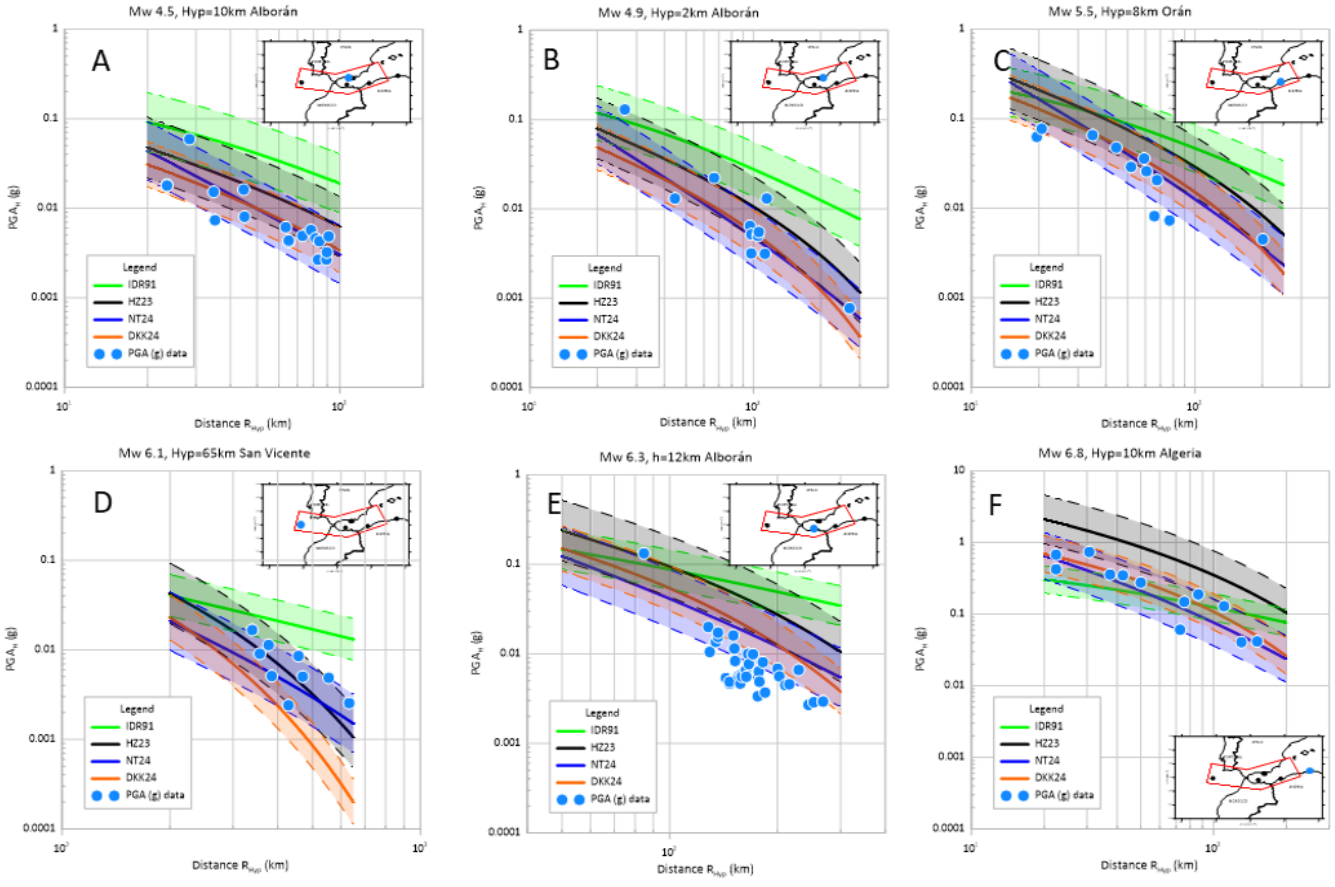

Figure 4. Relationship plots between PGA (g) and hypocentral distances (R_{Hyp}) of the selected GMPEs. Solid lines denote the median prediction curves for each earthquake, whereas the shadowed region between the dashed lines denote one standard deviation range ($\pm\sigma_\varepsilon$).

The predicted PGAs, through the HZ23, NT24 and DKK24 models and their respective standard deviation bands around each curve are consistent with the observed ones from the six tested earthquakes (Fig. 4). Most of the observed PGAs are within $\pm\sigma_\varepsilon$ bands. However, IDR91 behaves as an upper limit boundary of models in the majority of cases and, for M_w 6.3 Alboran Sea earthquake (Fig. 4 E), the observed PGAs are usually lower than the predicted values of the GMPEs for seabed. To evaluate the model's accuracy, residuals were obtained as the difference between the observed PGAs and the estimated PGA from the selected GMPE. As Fig. 5 shows, a near-zero tendency of residual distribution is found, with mean residual values presented in Table 3. Despite the oscillations discernible in the graphs (Fig. 5 A, C), residuals are situated between the curves (dashed lines in the graphs Fig. 5 A, C) that delineate the uncertainty bands ($\pm\sigma_\varepsilon$). The residuals demonstrate bounded variance homoscedasticity, with standard deviations of about 0.077 g, 0.236 g, and 0.047 g for IDR91, HZ23 and NT24, respectively, with the M_w 6.8 earthquake exception. All four GMPEs evaluated demonstrate adequate goodness of fit; however,

https://doi.org/10.5194/egusphere-2025-3248
Preprint. Discussion started: 12 September 2025

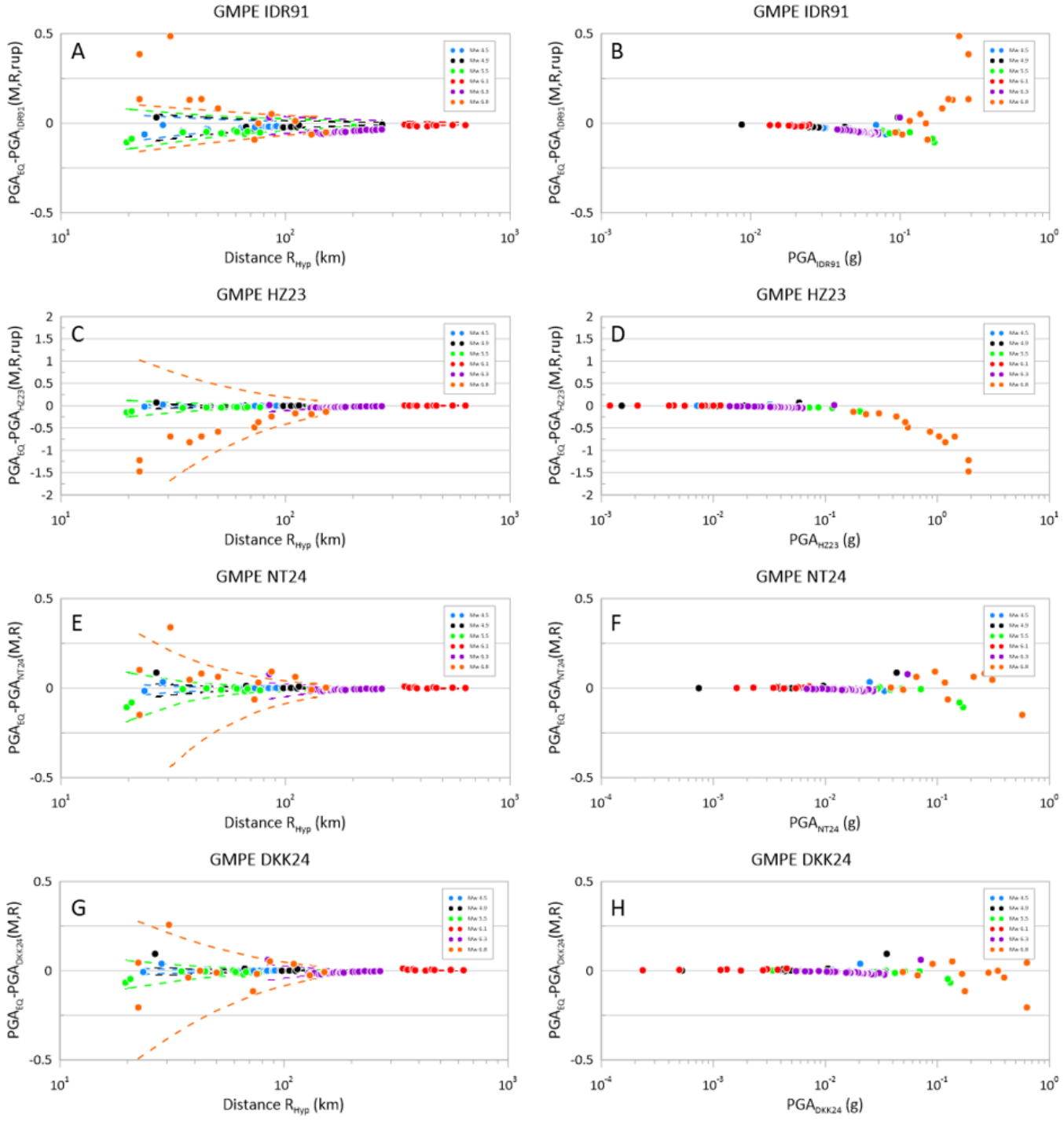

Figure 5. Residual plots of the goodness of fit for the predicted values by the selected GMPEs — IDR91, HZ23, NT24, and DKK24 — against the registered data in the earthquakes used for diagnosis.

https://doi.org/10.5194/egusphere-2025-3248
Preprint. Discussion started: 12 September 2025

NT24 and values that exceed the observed ones, with the exception of the closest recorded PGAs. The GMPE that exhibits a reduced capacity to capture this variability is HZ23 (see Fig. 5 C, D), with the highest RMSE (Table 3) relative to the others, but predicting a higher seismic intensity, according to the observed residuals, primarily for the largest earthquake (M_w 6.8). Its prediction is, in this instance, limited by the lower boundary curve of the uncertainty band of one σ_ε.

Table 3: Diagnosis of selected GMPEs.

GMPE	RES_{PGA} = Residuals of PGAs PGA_{EQ}-PGA_{GMPE}(M,R,rup)		ε = RES_{LogPGA} = Residuals of log PGAs Log(PGA_{EQ}-)-Log(PGA_{GMPE}(M,R,rup))		Standardised (RES_{LogPGA}) p-values – 95% confidence	
	Average	RMSE	Average ε	Std ε	Saphiro-Wilk	K-S
IDR91	-0.020	0.077	-1.4702	0.9012	0.00004	**0.09164**
HZ23	-0.090	0.236	-1.0494	0.7663 (0.723)	0.01057	**0.5848**
NT24	0.002	0.047	-0.1310	0.2855 (0.7784)	**0.21763**	**0.8160**
DKK24	-0.0043	0.040	-0.1267	0.3630 (0.377556)	0.000796	**0.2919**

The final step in the diagnosis undertaken here evaluates the properties of the prediction errors in the logarithms of the PGA (Fig. S1), as defined in Eq. (1). The averages of the epsilon values should be zero, where NT24 and DKK24 best fit the theoretical value (Fig. 6A). Their standard deviations are either below or very close to the values that the authors of the GMPEs provide for their models. Furthermore, it cannot be discarded that residuals in the logPGA have a normal distribution, as shown by the histogram for and the Q-Q plot (Fig. 6B, C) and indicated by the p-value for the Kolmogorov-Smirnov and the Saphiro-Wilk tests in NT24 (bold p-values in Table 3) at 95 % confidence.

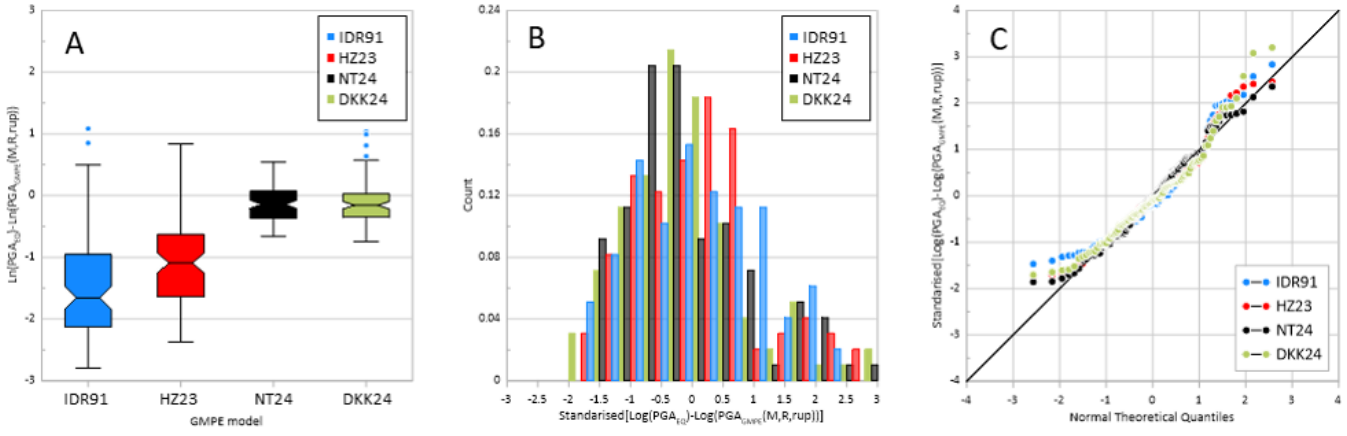

Figure 6. Diagnosis of the residuals in logarithms of PGA. A) Box-Whisker plot of residuals for each GMPE model used here. B) Stacked histogram in relative frequencies for the residuals in logarithms of PGA. C) Q-Q plot of the standardised residuals in logarithms of PGA.

https://doi.org/10.5194/egusphere-2025-3248
Preprint. Discussion started: 12 September 2025

4. Seismic hazard assessment

Seismic hazard refers to the probability of exceeding a certain earthquake intensity in a specific area within a given time period (Kijko, 2019; McGuire, 2004). Seismic hazard can be assessed using two main methods: Deterministic Seismic Hazard Analysis (DSHA) and Probabilistic Seismic Hazard Analysis (PSHA). In DSHA, hazard is defined as a specific percentile (such as the 50th, 84th, or 98th, as used in this study) of ground shaking intensity measured as peak ground acceleration (PGA) caused by one or several earthquakes. This method uses basic earthquake data and ground motion models based on a chosen earthquake scenario(Krinitzsky, 1995, 2002). Despite their deterministic character, the results obtained have frequently been used as a proxy for the upper limit of seismic intensity. Seismic hazard in PSHA is determined by calculating ground motion frequencies or exceedance rates using a mathematical model based on earthquake statistics and ground motion functions (McGuire, 2004, 2008). This model takes into account uncertainties related to earthquake size and moment (Kramer, 1996). PSHA methods can be categorized into parametric, using the total probability theorem (Cornell, 1968; Kramer, 1996), and nonparametric methods that utilize extreme value distribution functions (Epstein and Lomnitz, 1966). Other approaches, such as NDSHA, are often discussed together with DSHA and PSHA in relation to their representativeness for the largest events. Although both SHA methods use seismological and geological information, they define and calculate seismic hazard differently, which improves the understanding of seismic hazard forecasting at the studied site or region (Orozova and Suhadolc, 1999; Wang and Cobb, 2012).

4.1 Deterministic Seismic Hazard Assessment (DSHA)

The main input parameters in the classic DSHA (Reiter, 1990) are the maximum magnitude associated with the characteristic earthquake as the MCE for each seismic source area and a set of attenuation relationship or GMPEs. DSHA does not explicitly incorporate probability and recurrence functions, the seismic hazard is obtained as a certain percentile of ground motion. The 50th percentile is mostly used in preliminary DSHA studies, as well as the 84th percentile when it is used for inland critical structures such as nuclear or hydraulic power plants. Thus, some DSHA use the second quartile PGA plus a standard deviation, which is equivalent to an exceedance probability of 16% (Ben-Zion et al., 2003), calculated from simple earthquake and ground motion statistics (Krinitzsky, 1995, 2002). To perform these calculations, this work follows a series of steps as the classic DSHA scheme (Kramer, 1996; Krinitzsky, 1995; Reiter, 1990) that allow the deterministic derivation of the seismic hazard with a zone-based method:

(i) Build a catalogue of seismogenic sources $\{SS_j\}_{j = 1 \dots Nf}$.

(ii) Assign the seismic potential to each source SS_j with its MCE_j and the prevailing focal mechanism (normal, reverse or strike-slip).

(iii) Select the set $\{f^i\}$ of the empirical GMPEs or attenuation relationships $Y^i=f^i(M,R,\phi^i_k,\sigma^i_Y)$, with their corresponding parameters ϕ^i_k and the random uncertainties σ^i_Y for each i-th prediction equation.

https://doi.org/10.5194/egusphere-2025-3248
Preprint. Discussion started: 12 September 2025

(iv) Arbitrarily select the desired probability of exceedance $PR_{exed}=Pr[Y>=y_{max}/M,R]$, for a seismic scenario given by the (M,R) pair.

(v) Calculate the p-th percentile equivalent to the probability of exceedance:

$$PC_{Pr}= Pr[Y<y_p/M,R]=1- Pr[Y>=y_p/M,R] \quad (2)$$

(vi) Calculate the standard normal random variable Z_{01}, of mean 0 and variance 1, that matches the percentile PC_{Pr}.

(vii) Loop for each site P located at the geographic coordinate position (x,y,h) with latitude, longitude and hypsometry (height or depth above mean sea level) do,

(viii.a) Loop for each j-th seismic source SS_j (j=1,.... N_F), assuming that the worst-case scenario (M,R, focal mechanism) is selected, defined as the occurrence of an earthquake of magnitude M=MCEj from a point of the j-th seismogenic source at the shortest possible distance $R = R_{min} =min\{d(P,SSj)\}$, based on the distance to be handled (R_{JB}, R_{ep}, R_{hip}, etc.) in the attenuation function (Fig. 3).

(viii.a.1) Calculate the median ground motion (50th percentile or GMPE treated as deterministic) of the seismic parameter $Y^i_{50,j}$ at the site, with each i-th GMPE: $Y^i_{50,j} = f^i(M,R,\phi^i_k)$.

(viii.a.2) Calculate the p-th percentile of the seismic parameter at the site with the i-th equation of motion:

$$\log Y^i_{p,j} = \log Y^i_{50,j} + Z_{01}\, \sigma^i_Y \quad (3)$$

(viii.a.3) Obtain the on-site seismic ground shaking parameter $Y_{p,j}$ on site P produced by each j-th earthquake source.

(viii.b) Deterministic evaluation of the th-percentile of the seismic hazard $Y_p(x,y,h)$ at the site located at (x,y,h) as the largest parameter of the intensity of ground shake obtained from each seismogenic source: $Y_p(x,y,h) = \max\{Y_{p,j}\}$

(ix) Write $Y_p(x,y,h)$ output to change to a new location of the P site to assess.

However, since in each GMPE the logY value is distributed as a normal random variable of mean logY with standard deviation σ (Kramer, 1996), and $Y_p(x,y,h) = \max\{Y_{p,j}\}$, both Y_p and $Y_{p,j}$ are random variables. The p-th percentile Y_p is accurately calculated as follows:

$$\Pr\left[Y_p <= \frac{y_p}{M,R}\right] = F\left(\frac{\log Y_p - \log y_{max/M,R}}{\sigma}\right) = \frac{p}{100} \quad (4)$$

in accordance with the classical scheme, with a single dominant seismic source, and where F denotes the cumulative density function of the standard normal distribution (e.g., mean μ = 0, and variance = 1). Now, considering the distribution of $Y_{p,NS}$ as the extreme value of a set of values (Ang and Tang, 2007; Coles, 2001), the above approximation is computed as:

$$\Pr\left[Y_{p,NS} <= \frac{y_p}{M,R}\right] = \Pr\left[Y_1 <= \frac{y_p}{M,R}\right] x \Pr\left[Y_2 <= \frac{y_p}{M,R}\right] x \ldots x \Pr\left[Y_{NS} \le \frac{y_p}{M,R}\right] = \frac{p}{100} \quad (5)$$

https://doi.org/10.5194/egusphere-2025-3248
Preprint. Discussion started: 12 September 2025

This implies incorporation of the effect of the remaining NS seismic sources in the hazard percentile estimation in the hazard assessment. The estimation is more complicated than in the case of a single source, as it is now necessary to solve the nonlinear equation:

$$\prod_{j=1}^{NS} F\left(\frac{\log Y_{p,NS} - \log y_{j/M,R}}{\sigma}\right) = \frac{p}{100} \quad (6)$$

As this paper uses an approach based on a logic tree scheme that weights the GMPEs to capture the epistemic uncertainties in the hazard estimation, the above equation is rewritten to solve for each i-th GMPE $f^i(M,R,\phi^i_k)$ used and its corresponding i-th random uncertainty σ^i:

$$\varphi^i\left(\log Y^i_{p,NS}\right) = \prod_{j=1}^{NS} F\left(\frac{\log Y^i_{p,NS} - \log y_{j/M,R}}{\sigma^i}\right) - \frac{p}{100} = 0 \quad (7)$$

from which each $Y^i_{p,NS}$ is obtained.

4.2 Probabilistic Seismic Hazard Assessment (PSHA)

The principles of PSHA find their roots in the work of Cornell (1968) and Cornell et al. (1971), programmed in FORTRAN by McGuire (1976) at the USGS. To this end, Cornell proposes a probabilistic method whereby, having established the probability relationships that govern seismic events in a seismogenic area (point, fault plane, or spatial region) regarding the distribution of locations, sizes, and recurrence times, and knowing the past seismicity of the area (Benito and Jiménez, 1999), it is possible to quantify the probability of exceeding a specific level of ground motion at least once in that area over a specific exposure time (Kijko, 2019) using the total probability theorem (Kramer, 1996).

The technique for carrying out PSHA is described in several steps (Kramer, 1996; McGuire, 2004; Reiter, 1990):

(i) identification and characterization of seismic sources;
(ii) determination of the recurrence distribution of each source, in time or magnitude;
(iii) establishing the response parameter based on magnitude, distance, and site conditions with its uncertainty; and
(iv) calculating the probability that the response parameter is exceeded over a time period and estimating the hazard at the studied site, resulting from the sum of the hazard probabilities of all seismic sources influencing it.

https://doi.org/10.5194/egusphere-2025-3248
Preprint. Discussion started: 12 September 2025

This method allows for obtaining the mean annual exceedance rate ($\lambda_{IM>x}$) for a given site and exposure time, defined as the probability that a specified level x of intensity measure (IM) of ground motion is exceeded at this site (McGuire, 2004):

$$\lambda_{IM>x} = \sum_{i=1}^{N_S} v_i \int_{r=0}^{\infty} \int_{m=M_{min}}^{M_{max}i} P[IM > x|m,r] f_{Mi}(m) f_{Ri}(r)\, dm\, dr \quad (8)$$

Where:

- $\lambda_{IM>x}$ is the annual exceedance rate of a soft soil movement intensity IM that exceeds a threshold value x.
- $P[IM > x|m,r]$ is the probability that IM exceeds x given an earthquake of magnitude M= m at a distance R= r.
- $f_{Mi}(m)$ is the probability distribution of the earthquake magnitude.
- $f_{Ri}(r)$ is the probability distribution of the distance to the site.
- N_s is the total number of seismic sources considered.

And the mean annual occurrence rate of earthquakes from source i:

$$v_i = \exp(\propto_i - \beta_i m_0) \quad (9)$$

with $\alpha = a \ln(10)$ and $\beta = b \ln(10)$ being the parameters of the Gutenberg-Richter recurrence law:

$$\lambda_m = \exp(\alpha - \beta m) = 10^{a-bm}, \quad (10)$$

adjusted from the seismic catalog of the project using statistical techniques of least squares or maximum likelihood. The probability function in (8) is:

$$P[IM > x|m,r] = 1 - F_{IM}(x) = 1 - \Phi'\left(\frac{\ln x - \ln IM_{average}}{\sigma_{\ln_{IM}}}\right) \quad (11)$$

where the function $P[IM > x \mid m,r]$ indicates the IM ground motion parameter generated by a source i of magnitude (m), distance (r), and uncertainty epsilon (ε) in relation to the threshold value x. Finally, $f_{Mi}(m)$ and $f_{Ri}(r)$ are the parametric probability density functions for which a functional model is assumed, estimated from the magnitude and distance catalogue.

Results are expressed as seismic hazard curves (SHC), which can be obtained for different intensity measures, the most common being Peak Ground Acceleration (PGA), representing the exceedance probabilities over usually 50 years, and the ordinates of the acceleration spectrum $S_a(T)$. Another result is the response spectra, commonly referred to as uniform hazard spectra (UHS), derived from the SHC and obtained for each chosen return period.

https://doi.org/10.5194/egusphere-2025-3248
Preprint. Discussion started: 12 September 2025

4.3 Epistemic uncertainty treatment: logic tree scheme in DSHA and PSHA

There are numerous uncertainties in the DSHA and PSHA methodologies that arise from limited comprehension of the seismic process. The random nature of earthquakes and their occurrence generates variations in the spatial, temporal, and magnitude distribution when defining and characterizing seismic sources. In addition, the way seismic waves attenuate as they propagate from the source to the site of interest can be uncertain, generating uncertainties about the attenuation models or GMPEs, whose statistical adjustment of their coefficients incorporates an estimation error. Moreover, the arbitrary choice of GMPEs by users is itself an unsure process. All these uncertainties can be classified as random and epistemic (Kiureghian and Ditlevsen, 2009; McGuire and Shedlock, 1981).

In this work, the logic tree method has been used as a practical method to incorporate and analyse the inherent uncertainties both for DSHA and PSHA analysis. Its formulation uses weighting factors, assigned to seismic source models and GMPEs based on their likelihood (Coppersmith and Youngs, 1986; EPRI, 1987). The logic tree is constructed from a series of branches connected through nodes, from which the computational process twigs according to a possibility or appropriate weighting factors $\{w^i\}$. These factors are assigned based on expert judgment (Budnitz et al., 1997), depending on the suitability and importance of each seismic source model and GMPE used. The treatment of uncertainties by the logic tree scheme is made mathematically explicit in the calculation process in the equations to obtain $Y_{p,j}$ at site P produced by each j-th seismic source:

$$Y_{p,j} = \Sigma_i \, w^i \, Y^i_{p,j}$$

And also, to obtain $Y_{p,Ns}$ at each site P:

$$Y_{p,Ns} = \Sigma_i \, w^i \, Y^i_{p,Ns}$$

which includes the effects of the N_S seismic sources. The logic tree scheme shown here is used both for the estimation of the PGA based on a single control source, with the most unfavourable seismic scenario, and for the PGA estimation based on all seismogenic sources with their particular seismic scenario.

The logic trees used in this study incorporate a combination of three seismic source models and three GMPEs, selected to estimate the PGA in our study area. In the logic trees used in the DSHA (Fig. 7a) and PSHA (Fig. 7b), the weights assigned to each seismic source model were those used in the ESHM20 (Danciu et al., 2024). In contrast, each GMPE was implemented independently in this study, so the weighting assigned to each GMPE in the logic tree was unitary, generating three different seismic hazard results.

https://doi.org/10.5194/egusphere-2025-3248
Preprint. Discussion started: 12 September 2025

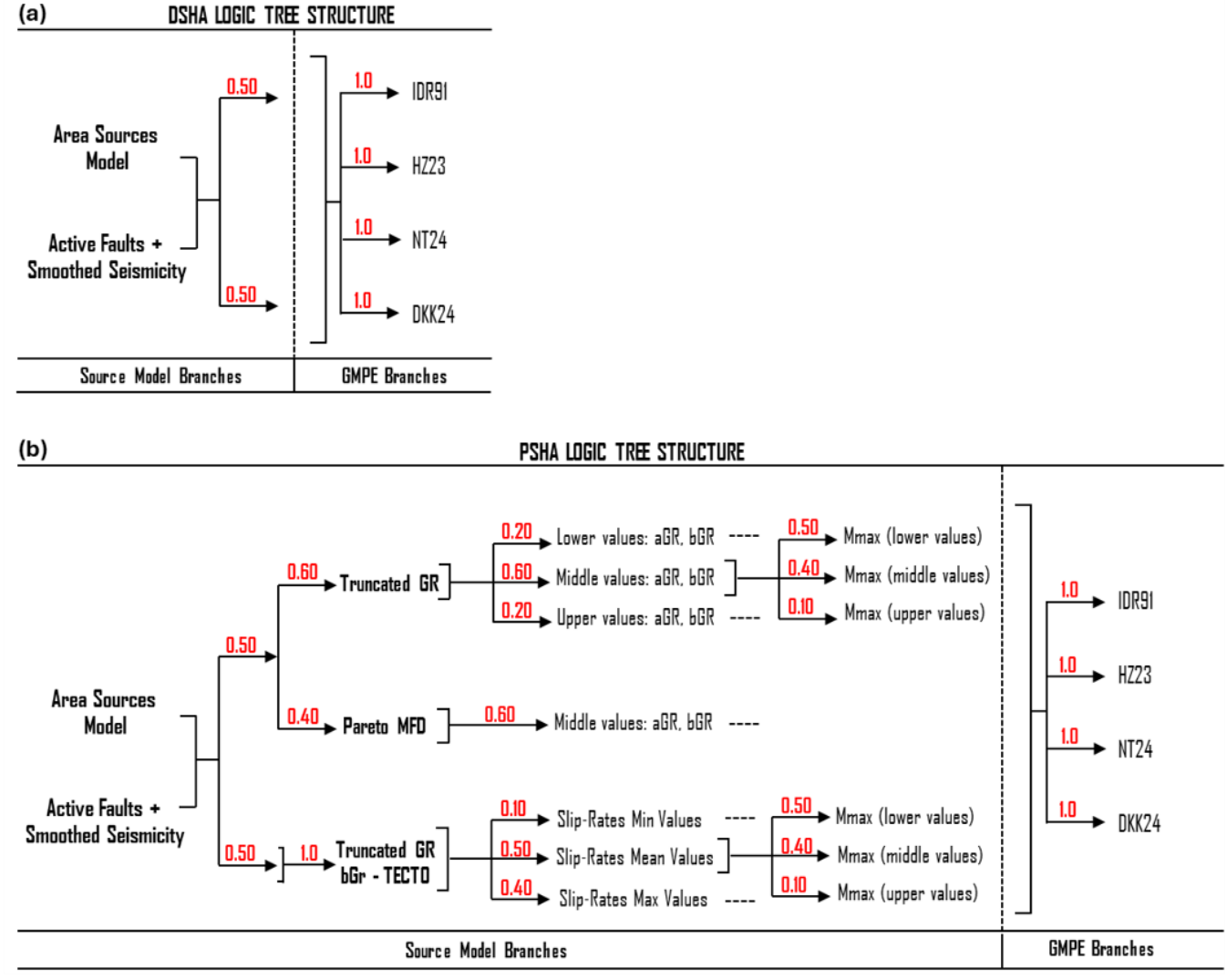

Figure 7. Schematic representation of the logical tree structure of the seismic hazard models: (a) DSHA and (b) PSHA. The weights assigned for each branch are shown in red. (modified from Danciu et al., 2024).

4.4 DSHA and PSHA calculation specifications

The open source DTM downloaded from EMODnet website (Fig. 1) has been used to generate the computational grid in the seismic hazard calculations of this work. The DTM was resampled to generate grid points spaced at 0.1 degrees (approximately the standard error in earthquake epicentre determination; Panza et al., 1990). In addition to its geographical coordinates, each point was assigned its respective bathymetric or topographic elevation. This mesh size, commonly used in the region (e.g., Danciu et al., 2024; IGN-UPM, 2017; Poggi et al., 2020), was chosen for its balance between computational efficiency and spatial resolution. This allowed capturing the variations in seismic hazard in this study while keeping a

https://doi.org/10.5194/egusphere-2025-3248
Preprint. Discussion started: 12 September 2025

manageable computational load. Thus, computationally, SHA calculations, using DSHA and PSHA, were performed on a grid of 3,854 sites (Fig. S2). The vertical component that the DTM incorporates is used in the estimation of the relative geographical distances, from the site to the seismogenic source, used by some of the GMPEs.

For DSHA calculations, a MATLAB© code has been developed to calculate the seismic intensity with a selected GMPE, from different seismic source types, incorporating the extreme value distribution into the DSHA as the scenario in which all seismic sources contribute (maximum Y distribution in Eq. (5)), and to account for the logical tree with them. Since the extreme value distribution must be determined at each site where the hazard is estimated, the convergence characteristics of this algorithm allow it to be repeated for up to 100 iterations. This number is sufficient to achieve an admissible error, |Xo - X*| in the root X* solution of Eq. (7) (Burden et al., 2015). Moreover, to notably reduce the computational time compared with older DSHA versions (e.g., Wang et al., 2012), the algorithm has been improved by its parallelization in MATLAB©º (R2024a, Update 6, available at https://www.mathworks.com, last accessed: 08/07/2025).

PSHA calculations provided for the mean values of PGA (in g) and four annual probabilities of exceedance (APEs), i.e., 0.01, 0.002105, 0.000404, and 0.0002, which correspond to the return periods of 100, 475, 2475, and 5000 years, respectively. These hazard maps are prescribed in the European seismic-resistant standards. Here, the OQ Engine configuration and the input files used are publicly available from ESHM20 (Danciu et al., 2021b, c), but the calculations were performed under soft soil conditions, with a Vs30 = 200 m/s, corresponding to class E according to the Eurocode 8 classification (CEN, 2004) and the National Earthquake Hazards Reduction Program (NEHRP) (BSSC, 2004). The DTM was incorporated into the calculations. For epistemic uncertainty representation in this study, a total of 100,000 logic trees end-branches were sampled using the OQ random technique. The programming of the new GMPEs, as well as all PSHA calculations in this study, was carried out using OpenQuake (OQ) engine (Pagani et al., 2014) version 3.21.0 in development mode (available at https://docs.openquake.org/oq-engine/manual/3.19/getting-started/installation-instructions/universal.html#devel-installation, last accessed: 08/07/2025).

5. Seismic Hazard assessment results and discussion.

The findings of this study demonstrate the effectiveness of using both DSHA and PSHA methodologies to generate seismic hazard maps within the IMR. These maps are based on the most recent GMPEs specifically tailored for offshore environments and show statistically robust compatibility with the available seismic data. This advancement represents a significant improvement over previous results in this field. In particular, this study extends and updates the only published maps (i.e., Molina Palacios, 1998) in the IMR.

The seismic hazard maps presented in the results obtained with either DSHA or PSHA suggest that the highest PGA values are concentrated in deep seafloor areas, where areal seismogenic sources of medium and high activity and faults are found. It has been demonstrated in previous studies that PGA maps depict the areas of highest seismic intensity as being limited to

https://doi.org/10.5194/egusphere-2025-3248
Preprint. Discussion started: 12 September 2025

coastal and inland regions of the Iberian Peninsula and northern Africa or zones characterized by high seismic activity along major tectonic fault line (e.g., Danciu et al., 2024; IGN-UPM, 2017; Poggi et al., 2020). However, the present results expand the geographical coverage of previous studies by highlighting the overlapping influence of the Gorringe and Horseshoe active zones with the SVF, MPF, and SWIM faults (distributed across the western IMR) and by emphasizing the significant role of the Arzew, AIF, and YSF faults in shaping the diffuse seismicity sources in the Alboran Sea. This is of great interest in the design of offshore infrastructures and their current and future deployment on the ocean floor, as vulnerable infrastructures may be affected by significant seismic effects not previously considered (Karthigeyan, 2022; Kee et al., 2023). The seismic intensity of these effects varies according to the approach used for the SHA and the soft ground attenuation function applied. However, a discernible amplification is evident in all cases when compared to equivalent PGA maps on comparable rock formations in emerged zones bordering the IMR of this study or in seafloor zones.

5.1 Probabilistic approach

The seismic hazard maps for the area between the western Gulf of Cádiz and the eastern Alboran Sea, with return periods of 100, 475, 2475, and 5000 years are shown in Figure 8. The maximum expected PGA values depend significantly on each GMPE used, thus generating four different seismic hazard scenarios in the IMR. Using IDR91, the mean horizontal PGA values reach 0.39 g, 0.60 g, 0.91 g and 1.06 g, for each the analysed return period. With NT24, these values reach 0.72 g, 1.78 g, 2.43 g and 2.90 g. It is considered that the results obtained with HZ23 model should be disregarded, considering the obtained PGA is greater than 3 g for most of the return periods; hence, suggesting numerical saturation of the model. In the case of the DKK24, maximum PGA values are around 0.51 g, 0.78 g, 1.06 g and 1.17 g, respectively. As commented, the range of PGA values in Figure 8, for the four seismic hazard scenarios presented, falls within the maximum values indicated for each return period. For each map shown, the highest PGA values are found in geographic areas over deep submarine zones of the IMR that exhibit the highest levels of seismic activity and intensity. Consequently, the highest seismic hazard values in the IMR are observed across most of the studied extent of the Gulf of Cádiz. This pattern is primarily attributed to deep seismic sources, located at approximately 60 km depth, which are associated with more intense reverse or strike-slip faulting ruptures. Notable among these area sources PTAS390, ESAS129, and MASS344 (identified in the ESMH20 catalogue) within the Gorringe and Horseshoe regions. Shallower right-lateral (RL) and reverse (RR) faults, including the SVF, MPF, and SWIM, also contribute to the observed hazard levels. In the Alboran Sea, the highest PGA values are mainly organised in accordance with the most active shallow fault systems, Arzew, AIF and YSF, forming a pattern of strike-slip oriented regions. It is evident that these values exhibit a reduced sensitivity to the selected GMPEs, in comparison to those obtained in the western sector of the Gulf of Cádiz. The PGA values, attributable to the AIF surface faults, are located over a SW-NE band that traverses the Alboran Basin and extends northwards, accompanied by a band of more attenuated intensities NW-SE, as a consequence of the YSF faults' orientation. At the easternmost point of the IMR, the Arzew Faults, which are characterised by elevated levels of activity, delineate a high-hazard zone along the Algerian coast that extends in an east-west direction, reaching almost the centre of the Alboran Basin. This phenomenon is attributable to the geometrical configuration of these semi-deep faults.

https://doi.org/10.5194/egusphere-2025-3248
Preprint. Discussion started: 12 September 2025

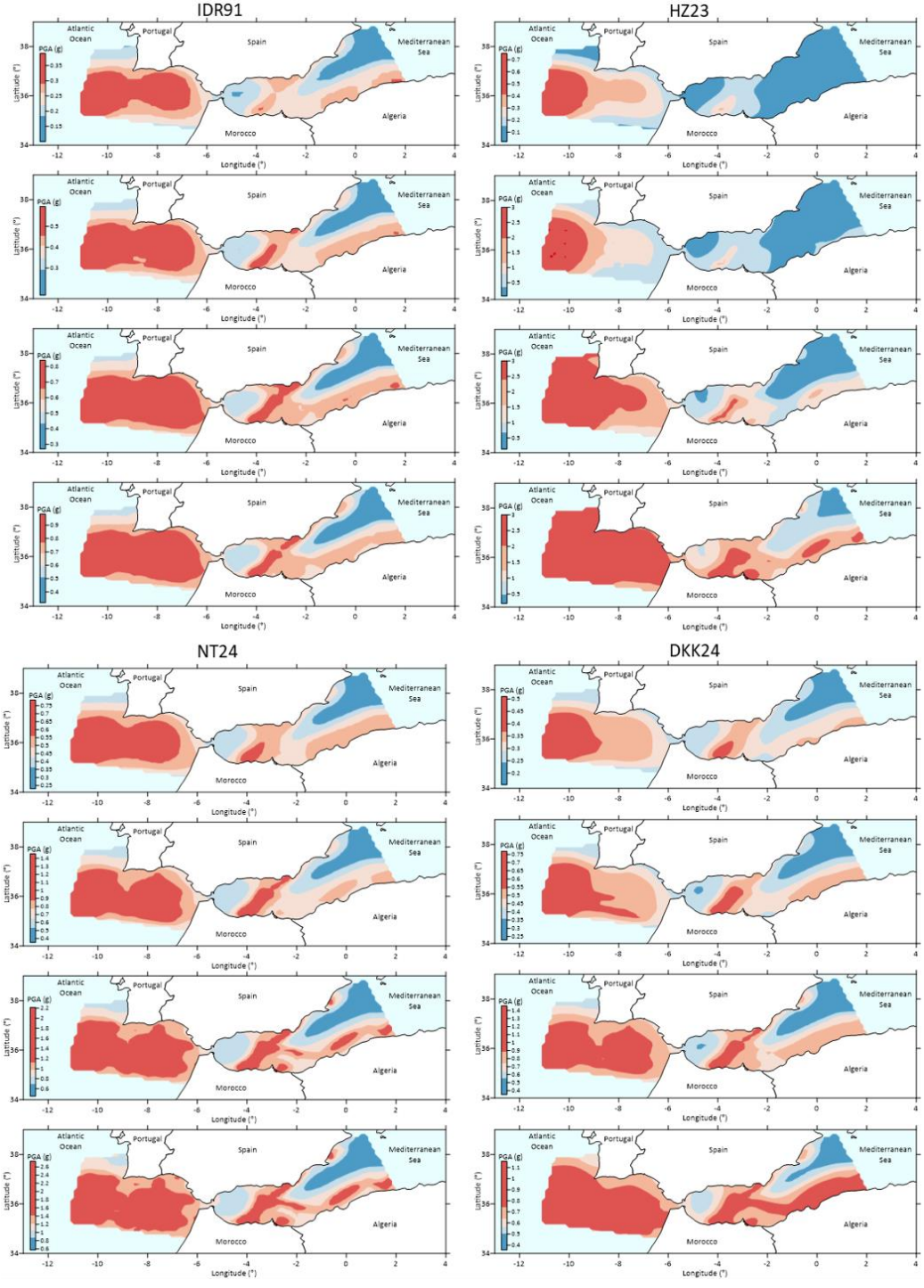

Figure 8. Probabilistic seismic hazard maps for the mean horizontal PGA (g) at APEs of 1/100, 1/475, 1/2475, and 1/5000, according to each GMPE used in this study. All values are estimated under soft soil conditions with Vs30 = 200 m/s.

https://doi.org/10.5194/egusphere-2025-3248
Preprint. Discussion started: 12 September 2025

Regarding the anomalously high PGA values (>3g) after the HZ23 model, it is likely that these results stem from extrapolating the model beyond its intended range of applicability. This extrapolation may lead to unrealistic ground motion estimates, especially when compounded by the relatively high standard deviation of the model ($\varepsilon = 0.7784$), and the absence of empirical calibration for the unique seismotectonic and geomechanical conditions of the IMR. The overprediction observed in the HZ23 results in the probabilistic and deterministic hazard maps suggests that, while the model may offer valuable insights within its original context, its use in the IMR should be approached with caution.

Results show significant differences compared to previous PSHA studies in the IMR (e.g., Molina Palacios, 1998), particularly in marine zones. These results not only refine previous assessments in IMR but also improve the understanding of the tectonic influence on offshore seismicity. More recent SHAs typically highlight the higher seismic intensity in the coastal areas of the Iberian Peninsula and North Africa (e.g., Danciu et al., 2024; IGN-UPM, 2017; Poggi et al., 2020). However, these new results extend the geographical scope of seismic hazard studies in the region by demonstrating considerable seismic activity in the marine areas of the IMR. This emphasizes the need to consider seabed seismic dynamics in regional SHA studies. The resulting seismic hazard maps could be highly valuable for offshore infrastructure design, as they highlight the potential vulnerability of current and future subsea facilities in the region.

5.2 Deterministic approach

The obtained mean PGA (g) seismic hazard maps (Fig. 9), considering the distribution of maximum control scenarios at each of the 3,854 study sites (Fig. S2), were generated by incorporating the DTM into the calculation, as well as the specific rupture mode of each fault and seismogenic source (Tables S1 and S2) and the GMPEs considered in this study: IDR91, HZ23, NT24, and DKK24. As illustrated in the applied logic tree (Fig. 7A), the implementation of each GMPE has resulted in a different seismic hazard scenario. Figure 9A shows the seismic hazard map considering IDR91. In this scenario, maximum PGA reaches around 0.91 g. With HZ23 (Fig. 9B), the maximum estimated PGA values exceed 3 g; hence HZ23 was disregarded. With NT24 (Fig. 9C), maximum PGA are of about 1.4 g. In contrast, when using DKK24 (Fig. 9D), maximum PGA values hover around 1.8 g.

For the four scenarios presented, the spatial distribution of accelerations shows relative similarities. The highest PGA values are found in the Gorringe seafloor and extend to the Horseshoe Plain in all four resulting maps. These abyssal areas are influenced by seismogenic sources and faults with moderate to strong seismicity, generating PGA outliers in the area, ranging approximately between 0.65 g and 1.8 g, excluding the previously discarded HZ23 results. To the west, PGA values range from 0.46 g to 1.2 g. This relates to a sequence of moderate seismicity sources along the Algerian coastal zone, together with the Arzew faults. Notably, the use of a DTM to determine the three-dimensional location of each calculation site, may result in amplified PGA values in areas where the site depth is closer to the seismic source, particularly in the deeper oceanic regions

https://doi.org/10.5194/egusphere-2025-3248
Preprint. Discussion started: 12 September 2025

of the IMR. In general terms, the PGA (g) maps obtained show a geographical distribution of the maximum values over the Atlantic areas of Gorringe, Horseshoe and Coral Patch, as well as off the Algerian coast, in the Mediterranean Basin of the Alboran Sea. This coincides with the areas of highest seismogenic potential in the IMR.

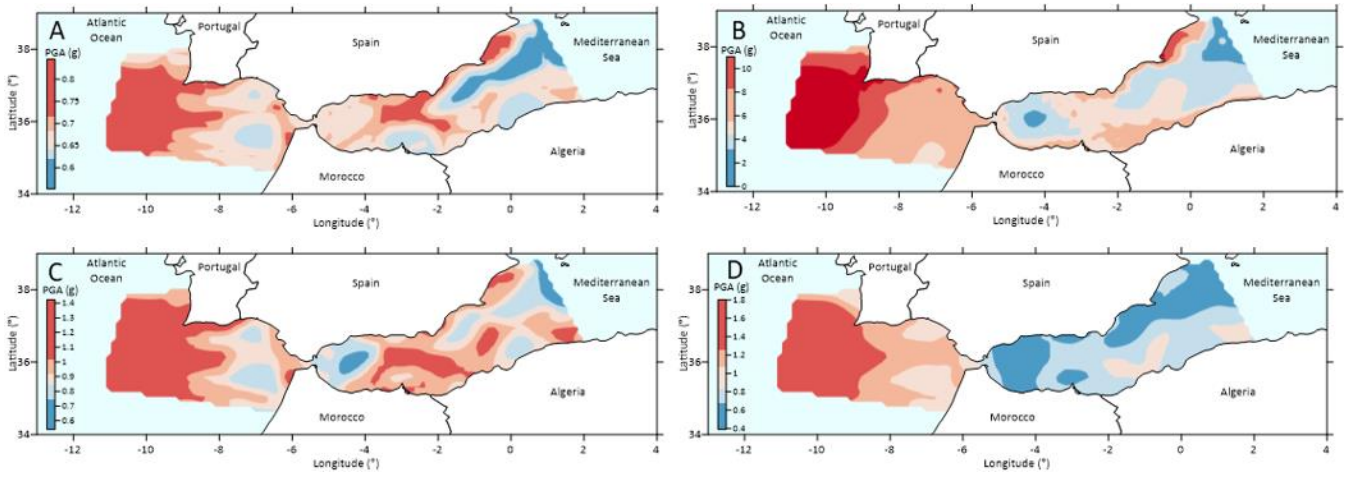

Figure 9. Deterministic seismic hazard maps in terms of mean PGA (g) under soft soil conditions, for the GMPEs used in this study: A) IDR91, B) HZ23, C) NT24, and D) DKK24.

The geographic distribution of the maximum expected PGA values obtained with the PSHA is very similar to the results obtained with the DSHA. As Reiter (1990) points out, the DSHA does not contemplate the inherent uncertainty in the estimation of seismic hazard, since the frequency of occurrence and magnitudes are not explicitly considered. So, a less accurate version, distributing the uncertainty due to randomness in the attenuation functions over a large region, is preferable, even though it provides larger values as in this work. These PGA values can be used as preliminary upper bounds of those that can be achieved, for different exceedance probabilities, rather than working with more precise, but less accurate PGAs.

The decision for the SHA method is based on its suitability for assessing earthquake hazards, as earthquakes are inherently random and unpredictable. It is important to acknowledge that hazard estimates cannot be fully verified due to the nature of seismic events (Musson, 2012a, b; Wang, 2012). Therefore, the use of DSHA could be recommended for critical industrial facilities of socioeconomic relevance.

5.3 Convergence in return period

The hazard maps obtained from deterministic and probabilistic estimations demonstrate a clear correlation: as the return period increases, PGA values calculated by PSHA increase and approach those obtained via DSHA. This finding corroborates the preliminary supposition that the results derived from the application of deterministic methodologies can be utilised as an upper limit on those derived from probabilistic methodologies. reinforcing the idea that DSHA may well be considered a

https://doi.org/10.5194/egusphere-2025-3248
Preprint. Discussion started: 12 September 2025

'worst-case' estimate of ground motion for a given earthquake scenario (Wang, 2011). Nevertheless, this assertion is supported by evidence to a certain degree. For lower exceedance probabilities, the hazard curve exhibits a monotonically increasing, quasi-asymptotic trend. As a result, beyond a certain return period, estimates using DSHA are surpassed. In the IMR, for 2475 years return period, a prominent 1:1 correlation is observed between the deterministically and probabilistically obtained PGA values (Fig. 10). The correlation structure between the two PGA values is dependent on depth, with the shallowest depths, i.e., those below 2500 m, exhibiting the poorest correlation and greatest dispersion. The correlation is most evident when using NT24 (Fig. 10 C), followed by IDR91 (Fig. 10 A) and finally DKK24 (Fig. 10 D). HZ23 (Fig. 10 B) has been excluded due to model saturation. For each GMPE, the correlations are more significant and show lower dispersion around 1:1 at the highest PGAs and over points at medium and high depths, above 2,500 to 3,000 m. The DSHA may underestimate or overestimate seismic hazard, causing this dispersion, in regions with complex or poorly understood seismic sources. In areas where there are multiple faults or where the seismic source zone or the maximum credible earthquake is uncertain (as is the case in this submarine area with scarce direct seismic data), the method may fail to account for all possible earthquake scenarios (Wang, 2011). The dispersion in PSHA is due to this method is highly dependent on the quality of the seismic catalogue, the GMPEs used, and the seismicity parameters (Peresan et al., 2013).

The correlation can be enhanced by combining expert knowledge with specific seismic intensity data from the region. This approach involves fine-tuning weights in the logic tree, which leads to an asymptotic quasi-equivalence between the results obtained with PSHA at larger return periods and those of DSHA. The efficiency and speed of DSHA calculations can serve as a preliminary approximation to SHA in scarce strong shake data areas. However, it is important to note that this claim cannot be made for all the GMPEs used, and it is not the aim of this paper to identify how the maximum correlation between the DSHA and PSHA approximations used here is achieved. With regard to the selection of the attenuation model, while the evaluation of the models in use does not provide statistical justifications for their rejection, the utilisation of solely the available recorded data from six significant offshore earthquakes did not adequately represent the anticipated behaviour across the entire IMR. In particular, it has been determined that HZ23, despite a favourable statistical diagnosis, yields PGA values that are considered too high (PGA > 3g) in comparison to those that would be observed in the area for a return period of 2475 year. Consequently, the PSHA calculations result in overestimated PGA values in certain regions of the IMR, despite these areas were not excluded during the preceding statistical validation tests.

https://doi.org/10.5194/egusphere-2025-3248
Preprint. Discussion started: 12 September 2025

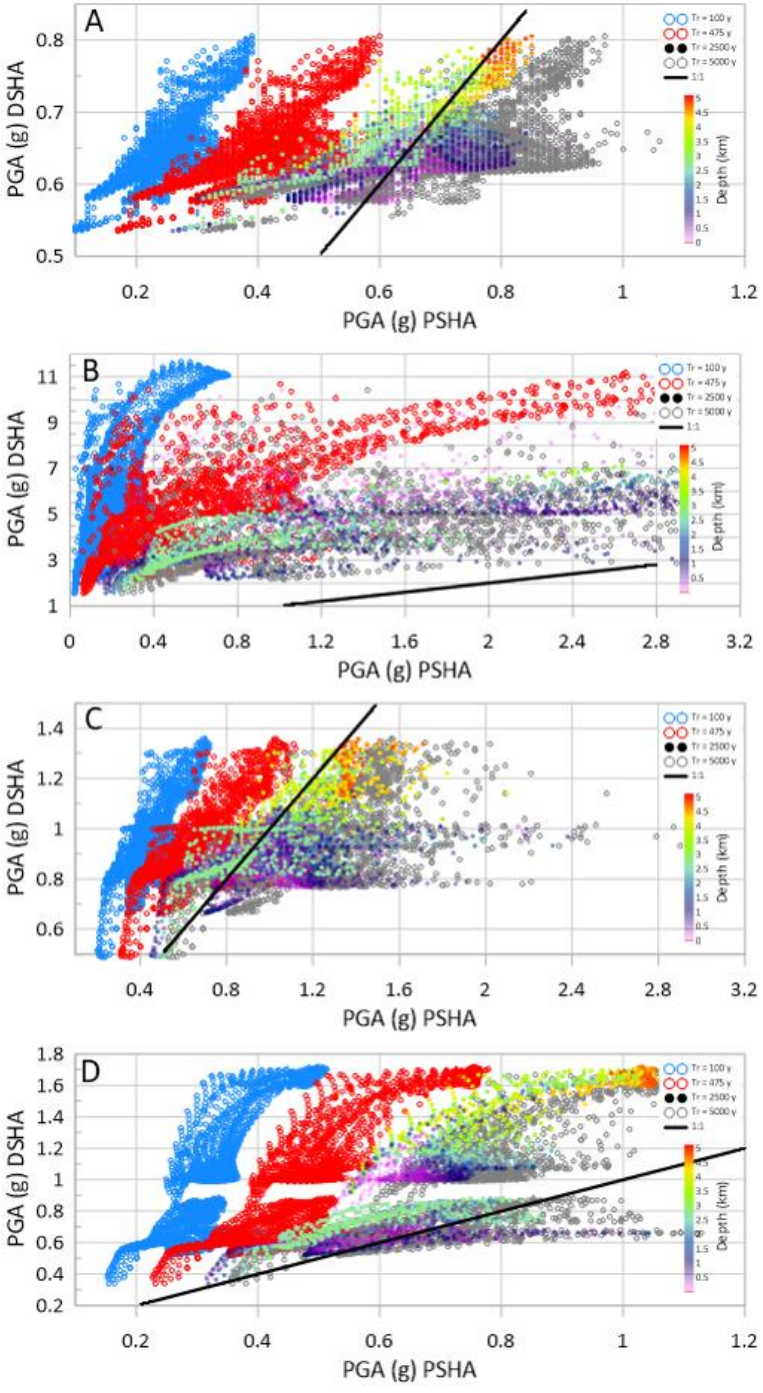

Figure 10. Scatter plots of PGA by DSHA vs. PGA by PSHA for the 100, 475, 2475, and 5000-year return periods for the GMPEs used in this work: A) IDR91, B) HZ23, C) NT24, and D) DKK24. Dots representing the 2475-year return period were colour-coded according to DTM depth.

https://doi.org/10.5194/egusphere-2025-3248
Preprint. Discussion started: 12 September 2025

5.4 Distribution of PGAs amplification in the ocean floor

The PGA values obtained using DSHA and PSHA with the GMPEs selected in this study, are higher than those obtained using input data files containing the information of the seismogenic sources (accessible via https://doi.org/10.12686/ESHM20-MAIN-DATASETS) and the OQ Engine configuration and input files (accessible via https://doi.org/10.12686/ESHM20-OQ-INPUT). These were used to calculate the ESHM20 hazard mapping scheme (Danciu et al., 2021a, 2024) in the IMR, as recorded in several ocean floor areas (Boore and Smith, 1999; Dhakal et al., 2021). The distribution of PGA values obtained by applying the ESHM20 is increased throughout its spectrum (Fig. 11 A) and with very similar rates for IDR91 and DKK24, and much higher for NT24. Incorporating the relief of the ocean floor through bathymetry has an effect, although not as significant as the amplification of the attenuation curves. The deeper the seismic intensity increases, the closer the control point is to the seismogenic sources in relation to inshore territory or mean sea level.

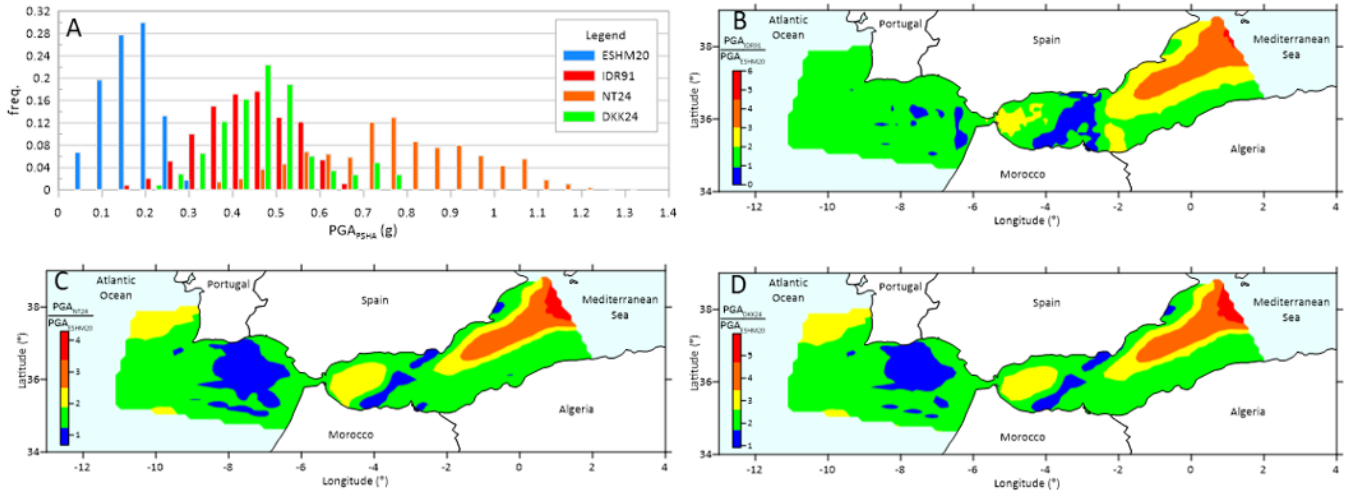

Figure 11. A) Histogram of the PGA values estimated by PSHA for a 475-year return period, from ESHM20, from different GMPEs and seismic models indicated in the legend. Relative amplification maps showing the percentage increment in estimated PGA values based on PSHA for each GMPE used in this work: B) IDR91, C) NT24, and D) DKK24.

The combination of GMPEs, bathymetry and the spatial distribution of seismogenic sources in this study has provided a new pattern of amplification rates PGA_{GMPE}/PGA_{ESMH20} (see Figs. 11 B-D). As demonstrated in the literature (see Dhakal et al., 2021; Hu et al., 2020), offshore sites exhibit differing distance attenuation when compared to inshore sites. This discrepancy is due to the incorporation of modifications to offshore zones as specified by the authors of the GMPEs within the model. It is acknowledged that some of the offshore GMPEs used (HZ23 and NT24) are derived from onshore GMPEs. The maximum amplification reaches approximately about 6 times PGA_{ESMH20} with IDR91 (Fig. 11 B), 4.5 times with NT24 (Fig. 11 C) and

https://doi.org/10.5194/egusphere-2025-3248
Preprint. Discussion started: 12 September 2025

about 5.5 times with DKK24 (Fig. 11D), all very specifically located in AOB. In the remaining zones, the rate of increase of the PGA is within the medium ranges in comparison to the reference PGA_{ESMH20} values in rock and emerged terrain (PGA at 475 years, calculated using the EMSH20 seismic model with the PSHA approach). It is observed that, in most of the studied area, the amplification rates were found to be less than double in all seismic hazard scenarios. The site effect is primarily attributable to the attenuation characteristics of soft seafloor soils and their depth found in WAB and AOB (Chen et al., 2023; Diao et al., 2014), which are incorporated through the GMPEs used.

There are notable similarities in the spatial distribution of PGAs amplification rates, regardless of the GMPE used. The highest amplification rates (represented by red and orange colors), exceeding five to six times max the PGA values from the ESHM20, are concentrated in regions where the expected PGA values are relatively low, such as the Argelo-Balearic Basin. Mid-range amplifications rates (green and yellow colors) are distributed across the entire study area. In this case, regions where the PGA values are already high, such as the Gorringe Ridge, Horseshoe Abyssal Plain, and the Algerian margin, the amplification rates tend to be moderate, typically ranging between 1.5 and 2.5 times the PGA_{ESHM20}. On the other hand, the lowest amplification rates (blue color) are observed in the West Alboran Basin (WAB), following the Alboran Ridge and Channel, as well as in the Gulf of Cádiz. As illustrated in these amplification maps, the phenomenon is most evident in the West Alboran WAB and the Algerian Ocean Basin (AOB), extending to the west in the Gorringe Ridge and Tagus Plain. In such instances, the site effect assumes a heightened significance, particularly in the context of basin bottoms characterised by the accumulation of substantial sedimentary deposits.

Within IMR geographical framework, no discernible spatial correlation is identified between the amplification outcomes resulting from the GMPEs used in this study. Areas exhibiting low seismic intensity, such as AOB, demonstrate a substantial amplification effect, while regions characterised by higher PGA values exhibit average amplifications, as observed in the Gorringe Ridge area, or even attenuations to the west of Gorringe Bank and in the AIF and YSF fields. Excluding these areas where the PGA values are highest or lowest, the study area shows an amplification rate of less than double, despite the variations in the PGA values obtained with the GMPEs used and with the ESHM20.

Due to the absence of data concerning strong motion events within the IMR, there exists inadequate empirical data within the magnitude-distance range to directly develop a GMPE using empirical regression techniques. The authors of this study argue that there is a significant need for underwater seismic observation stations. This need arises from the considerable uncertainty and limited understanding of attenuation processes within the IMR. This is despite the extensive knowledge already available on amplification and attenuation processes caused by the substantial water column and the rheological characteristics of the ocean floor. To address this gap, the authors recommend implementing underwater seismic stations similar to those used in the United States (Boore and Smith, 1999) and the S-Net network in Japan (Kanazawa, 2013).

https://doi.org/10.5194/egusphere-2025-3248
Preprint. Discussion started: 12 September 2025

This approach would enable two key advancements: 1) calibration and empirical modification of existing GMPE, as demonstrated in HZ23; 2) Reformulation of a regionally adjustable backbone attenuation function, or a system of ergodic functions, to better capture ground motion variability. Such methods have already been successfully applied in seismotectonic settings, as shown in the ESHM20 model (Kotha et al., 2020; Weatherill and Cotton, 2020). These improvements would be tailored to the specific Vs30 and D14 distribution characteristics of the IMR as recently detailed by Hu et al. (2024).

6. Conclusions

This study addresses the critical need for a comprehensive seismic hazard assessment in the IMR, particularly in the marine domain between the Gulf of Cádiz and the Alboran Sea. Despite the well-documented historical and instrumental seismicity of the region, previous hazard studies have largely focused on terrestrial zones, leaving a considerable gap in our understanding of undersea seismic hazard, especially in terms of PGA at the seabed level. This work contributes to filling that gap by applying both probabilistic (PSHA) and deterministic (DSHA) methodologies, adapted to offshore conditions and integrated with recent developments in seismogenic zonation (ESHM20) and GMPEs. This study has demonstrated that PGA estimation for seabed conditions is both feasible and meaningful, providing crucial insight for hazard mitigation planning in marine environments.

Key findings show that significant PGA values are present across deep marine zones of the IMR, particularly over the Gorringe Ridge, Horseshoe Plain, and along active fault zones near the Algerian margin. The results confirm a consistent spatial distribution of hazard for both DSHA and PSHA approaches, with maximum values occurring over regions characterised by dense seismogenic activity and structural complexity. Notably, the probabilistic results for long return periods (e.g., 2475 years) show convergence with deterministic outcomes, validating the use of DSHA as a robust upper-bound proxy in the absence of long-term probabilistic data, which may be particularly handy for infrastructures. The incorporation of four GMPEs (IDR91, NT24, HZ23, and DKK24) allowed a comparative analysis of offshore attenuation behaviour. Among these, NT24 and DKK24 provided the best statistical fit to observed regional ground motion data, while HZ23 exhibited overestimation tendencies beyond its intended magnitude range, indicating potential constraints in its application to this region. The logic-tree framework adopted in both DSHA and PSHA enabled the epistemic uncertainty to be systematically incorporated into the hazard modelling. The overestimation observed with HZ23 highlights the importance of developing or calibrating GMPEs specifically for the IMR, particularly for large magnitude, short distance offshore events. Given the extrapolation beyond the validated model range, we recommend that future SHA applications in the IMR down-weight HZ23 in the logic tree or exclude it of the analyses to avoid potential overestimation of PGAs in the region.

The findings have significant implications for the seismic design and risk management of subsea structures, such as pipelines, cables, wind farms, and potential transcontinental tunnels. Current hazard assessments based solely on terrestrial models may significantly underestimate seabed accelerations and associated risks in the IMR. Moreover, the results underscore

https://doi.org/10.5194/egusphere-2025-3248
Preprint. Discussion started: 12 September 2025

the importance of incorporating seabed-specific GMPEs and digital terrain models in offshore SHA, as bathymetry demonstrably affects source-to-site distances and thus ground motion predictions.

However, some limitations remain to be addressed. The scarcity of direct offshore strong-motion records and the use of a uniform Vs30 proxy to represent soft soils in the IMR required the adoption of GMPEs derived from analogue seismotectonic contexts, such as the Japan Trench. While this approach was statistically validated, it introduces uncertainties that should be addressed in future studies through the expansion of OBS monitoring networks in the region and region-specific GMPE calibration. Similarly, the DTM resolution, though consistent with regional studies, may benefit from refinement in areas of steep bathymetric gradients to improve hazard detail, accordingly, to include possible site-effects. Moreover, the potential interaction between earthquakes and co-seismic hazards (such as landslides and tsunamis) requires further research. This could be approached through integrated, multihazard assessment frameworks to better understand and manage these complex interdependencies.

The integration of Neo-deterministic SHA (NDSHA) methods and machine-learning approaches for source characterisation are promising avenues. The demonstrated alignment between DSHA and PSHA under appropriate modelling choices underlines the robustness of the results, offering a scientifically grounded tool for enhancing resilience in the face of submarine seismic risks in the IMR.

Code availability

MATLAB code from the corresponding author upon reasonable request. OpenQuake (OQ) engine code publicly available in https://www.globalquakemodel.org/product/openquake-engine.

Data availability

This work used publicly available ESHM20 datasets (accessible via https://doi.org/10.12686/ESHM20-MAIN-DATASETS and https://doi.org/10.12686/ESHM20-OQ-INPUT).

Author contributions

AJRB, CPB and MLLI: investigation. AJRB and CPB: conceptualization. AJRB and CPB: data preparation. AJRB and CPB: methodology. AJRB and CPB: software. AJRB and CPB: formal analysis. AJRB: writing (original draft). AJRB, CPB and MLLI: writing (review and editing). AJRB, CPB and MLLI: visualization. CPB and MLLI: supervision. MLLI: validation.

Competing interests

The authors have no relevant competitive or financial interests to disclose.

https://doi.org/10.5194/egusphere-2025-3248
Preprint. Discussion started: 12 September 2025

Acknowledgements

The authors would like to express their gratitude to João Fonseca and Alexandra Carvalho, whose suggestions helped improve and clarify this manuscript. We would also like to thank Dr. Laurentiu Danciu and Professor Giuliano Panza for their comments. The Open Access publishing for this study has been covered thanks to a CSIC agreement with Copernicus Publications. Thanks to the EMODnet Bathymetry Consortium (2020), EMODnet Digital Bathymetry (DTM) (https://doi.org/10.12770/bb6a87dd-e579-4036-abe1-e649cea9881a) to allow the download and use of the current EMODnet DTM version of December 2020, which has a resolution of 1/16 * 1/16 arc minutes.

References

AEIS-IGN: Seminario sobre criterios sísmicos para centrales nucleares y obras públicas: Madrid, 29-30 de marzo de 1978, Asoc. Esp. Ing. Sísmica AEIS Inst. Geográfico Nac. IGN, 1979.

Ang, A. H. and Tang, W. H.: Probability Concepts in Engineering Planning: Emphasis on Applications to Civil and Environmental Engineering, John Wiley and Sons, 2007.

Submarine Cable Map: https://www.submarinecablemap.com/, last access: 11 February 2025.

Atik, L. A., Abrahamson, N., Bommer, J. J., Scherbaum, F., Cotton, F., and Kuehn, N.: The Variability of Ground-Motion Prediction Models and Its Components, Seismol. Res. Lett., 81, 794–801, https://doi.org/10.1785/gssrl.81.5.794, 2010.

Ayadi, A. and Bezzeghoud, M.: Seismicity of Algeria from 1365 to 2013: Maximum Observed Intensity Map (MOI2014), Seismol. Res. Lett., 86, 236–244, https://doi.org/10.1785/0220140075, 2014.

Báez, J. C., Vázquez, J.-T., Camiñas, J. A., and Malouli Idrissi, M. (Eds.): Alboran Sea - Ecosystems and Marine Resources, Springer International Publishing, Cham, https://doi.org/10.1007/978-3-030-65516-7, 2021.

Barani, S., Albarello, D., Massa, M., and Spallarossa, D.: Influence of Twenty Years of Research on Ground-Motion Prediction Equations on Probabilistic Seismic Hazard in Italy, Bull. Seismol. Soc. Am., 107, 240–255, https://doi.org/10.1785/0120150276, 2016.

Basili, R., Danciu, L., Beauval, C., Sesetyan, K., Vilanova, S. P., Adamia, S., Arroucau, P., Atanackov, J., Baize, S., Canora, C., Caputo, R., Carafa, M. M. C., Cushing, E. M., Custódio, S., Demircioglu Tumsa, M. B., Duarte, J. C., Ganas, A., García-Mayordomo, J., Gómez de la Peña, L., Gràcia, E., Jamšek Rupnik, P., Jomard, H., Kastelic, V., Maesano, F. E., Martín-Banda, R., Martínez-Loriente, S., Neres, M., Perea, H., Šket Motnikar, B., Tiberti, M. M., Tsereteli, N., Tsironi, V., Vallone, R., Vanneste, K., Zupančič, P., and Giardini, D.: The European Fault-Source Model 2020 (EFSM20): geologic input data for the European Seismic Hazard Model 2020, Nat. Hazards Earth Syst. Sci., 24, 3945–3976, https://doi.org/10.5194/nhess-24-3945-2024, 2024.

Benfedda, A., Bouhadad, Y., Boughacha, M. S., Guessoum, N., Abbes, K., and Bezzeghoud, M.: The Oran January 9th (Mw 4.7) and June 6th, 2008 (Mw 5.4) earthquakes: Seismological study and seismotectonic implication, J. Afr. Earth Sci., 169, 103896, https://doi.org/10.1016/j.jafrearsci.2020.103896, 2020.

Benito, B. and Jiménez, E.: Peligrosidad sísmica, Física Tierra, 11, 13–47, 1999.

https://doi.org/10.5194/egusphere-2025-3248
Preprint. Discussion started: 12 September 2025

Ben-Zion, Y., Lee, W. H. K., Kanamori, H., Jennings, P. C., and Kisslinger, C.: Key formulas in earthquake seismology, Int. Handb. Earthq. Eng. Seismol., 81, 1857–1875, 2003.

Boore, D. M. and Smith, C. E.: Analysis of earthquake recordings obtained from the Seafloor Earthquake Measurement System (SEMS) instruments deployed off the coast of southern California, Bull. Seismol. Soc. Am., 89, 260–274, https://doi.org/10.1785/BSSA0890010260, 1999.

BSSC: NEHRP recommended provisions for seismic regulations for new buildings and other structures (FEMA 450). Part 1: Provisions., Build. Seism. Saf. Counc. BSSC Natl. Inst. Build. Sci. Wash. DC USA, 2004.

Budnitz, R. J., Apostolakis, G., and Boore, D. M.: Recommendations for probabilistic seismic hazard analysis: Guidance on uncertainty and use of experts, US Nuclear Regulatory Commission (NRC), Washington, DC (United States). Div. of Engineering Technology; Lawrence Livermore National Lab. (LLNL), Livermore, CA (United States); Electric Power Research Inst. (EPRI), Palo Alto, CA (United States); US Department of Energy (USDOE), Washington DC (United States), https://doi.org/10.2172/479072, 1997.

Buforn, E. and Udías, A.: Sismicidad y mecanismo focal de los terremotos de la región Cabo de San Vicente-Argelia, Rev. Soc. Geológica Esp., 20, 301–310, 2007.

Buforn, E., Sanz de Galdeano, C., and Udías, A.: Seismotectonics of the Ibero-Maghrebian region, Tectonophysics, 248, 247–261, https://doi.org/10.1016/0040-1951(94)00276-F, 1995.

Buforn, E., Udías, A., and Pro, C.: Large Earthquakes at the Ibero-Maghrebian Region: Basis for an EEWS, Pure Appl. Geophys., 172, 2387–2396, https://doi.org/10.1007/s00024-014-0954-0, 2015.

Buforn, E., Udías, A., and Pro, C.: Source mechanism studies of earthquakes in the Ibero-Maghrebian region and their tectonic implications, J. Seismol., 20, 1075–1088, https://doi.org/10.1007/s10950-015-9551-7, 2016.

Burden, R. L., Faires, J. D., and Burden, A. M.: Numerical Analysis, Cengage Learning, 918 pp., 2015.

Campbell, K. W. and Bozorgnia, Y.: Updated Near-Source Ground-Motion (Attenuation) Relations for the Horizontal and Vertical Components of Peak Ground Acceleration and Acceleration Response Spectra, Bull. Seismol. Soc. Am., 93, 314–331, https://doi.org/10.1785/0120020029, 2003.

CEN: Eurocode 8: design of structures for earthquake resistance—part 1: general rules, seismic actions and rules for buildings., Eur. Comm. Stand. CEN Bruss., BS EN 1998–1:2004: E, 219, 2004.

Chen, B., Wang, B., Ma, Z., Du, Y., and Li, C.: Influence of seawater depth on offshore ground motion characteristics and seismic responses of sea-crossing cable-stayed bridges, Ocean Eng., 280, 114853, https://doi.org/10.1016/j.oceaneng.2023.114853, 2023.

Chen, B., Wang, B., Hu, S., and Bi, K.: The influence of seabed on offshore ground motion, Soil Dyn. Earthq. Eng., 179, 108567, https://doi.org/10.1016/j.soildyn.2024.108567, 2024.

Chen, Y.-S., Weatherill, G., Pagani, M., and Cotton, F.: A transparent and data-driven global tectonic regionalization model for seismic hazard assessment, Geophys. J. Int., 213, 1263–1280, https://doi.org/10.1093/gji/ggy005, 2018.

Chester, D. K.: The 1755 Lisbon earthquake, Prog. Phys. Geogr. Earth Environ., 25, 363–383, https://doi.org/10.1177/030913330102500304, 2001.

https://doi.org/10.5194/egusphere-2025-3248
Preprint. Discussion started: 12 September 2025

Coles, S.: An Introduction to Statistical Modeling of Extreme Values, Springer, London, https://doi.org/10.1007/978-1-4471-3675-0, 2001.

Coppersmith, K. J. and Youngs, R. R.: Capturing uncertainty in probabilistic seismic hazard assessments within intraplate tectonic environments, in: Proceedings of the Third US national conference on earthquake engineering, 301–312, 1986.

Cornell, C. A.: Engineering seismic risk analysis, Bull. Seismol. Soc. Am., 58, 1583–1606, https://doi.org/10.1785/BSSA0580051583, 1968.

Cornell, C. A., Howells, D. A., Haigh, I. P., and Taylor, C.: Probabilistic analysis of damage to structures under seismic loads, Dyn. Waves Civ. Eng., 473–488, 1971.

Crespo, M. J., Martínez, F., and Martí, J.: Seismic hazard of the Iberian Peninsula: evaluation with kernel functions, Nat. Hazards Earth Syst. Sci., 14, 1309–1323, https://doi.org/10.5194/nhess-14-1309-2014, 2014.

Custódio, S., Lima, V., Vales, D., Cesca, S., and Carrilho, F.: Imaging active faulting in a region of distributed deformation from the joint clustering of focal mechanisms and hypocentres: Application to the Azores–western Mediterranean region, Tectonophysics, 676, 70–89, https://doi.org/10.1016/j.tecto.2016.03.013, 2016.

D'Acremont, E., Lafuerza, S., Rabaute, A., Lafosse, M., Jollivet Castelot, M., Gorini, C., Alonso, B., Ercilla, G., Vazquez, J. T., Vandorpe, T., Juan, C., Migeon, S., Ceramicola, S., Lopez-Gonzalez, N., Rodriguez, M., El Moumni, B., Benmarha, O., and Ammar, A.: Distribution and origin of submarine landslides in the active margin of the southern Alboran Sea (Western Mediterranean Sea), Mar. Geol., 445, 106739, https://doi.org/10.1016/j.margeo.2022.106739, 2022.

Danciu, L., Nandan, S., Reyes, C. G., Basili, R., Weatherill, G., Beauval, C., Rovida, A., Vilanova, S., Sesetyan, K., and Bard, P.-Y.: The 2020 update of the European Seismic Hazard Model-ESHM20: Model Overview, EFEHR Tech. Rep., 1, https://doi.org/10.3929/ethz-b-000590386, 2021a.

Danciu, L., Nandan, S., Reyes, C., Basili, R., Weatherill, G., Beauval, C., Rovida, A., Vilanova, S., Şeşetyan, K., Bard, P.-Y., Cotton, F., Wiemer, S., and Giardini, D.: Main Datasets of the 2020 Update of the European Seismic Hazard Model (ESHM20) [Data set], EFEHR Eur. Facil. Earthq. Hazard Risk, https://doi.org/10.12686/ESHM20-MAIN-DATASETS, 2021b.

Danciu, L., Nandan, S., Reyes, C., Wiemer, S., and Giardini, D.: OpenQuake Input Files for the 2020 Update of the European Seismic Hazard Model (ESHM20) [Data set], EFEHR Eur. Facil. Earthq. Hazard Risk, https://doi.org/10.12686/ESHM20-OQ-INPUT, 2021c.

Danciu, L., Giardini, D., Weatherill, G., Basili, R., Nandan, S., Rovida, A., Beauval, C., Bard, P.-Y., Pagani, M., Reyes, C. G., Sesetyan, K., Vilanova, S., Cotton, F., and Wiemer, S.: The 2020 European Seismic Hazard Model: overview and results, Nat. Hazards Earth Syst. Sci., 24, 3049–3073, https://doi.org/10.5194/nhess-24-3049-2024, 2024.

Dhakal, Y. P., Kunugi, T., Suzuki, W., Kimura, T., Morikawa, N., and Aoi, S.: Strong Motions on Land and Ocean Bottom: Comparison of Horizontal PGA, PGV, and 5% Damped Acceleration Response Spectra in Northeast Japan and the Japan Trench Area, Bull. Seismol. Soc. Am., 111, 3237–3260, https://doi.org/10.1785/0120200368, 2021.

Dhakal, Y. P., Kubo, H., and Kunugi, T.: Prediction Equations for Peak-Ground Accelerations and Velocities in Northeast Japan Using the S-net Data, J. Disaster Res., 19, 760–771, https://doi.org/10.20965/jdr.2024.p0760, 2024.

Diao, H., Hu, J., and Xie, L.: Effect of seawater on incident plane P and SV waves at ocean bottom and engineering characteristics of offshore ground motion records off the coast of southern California, USA, Earthq. Eng. Eng. Vib., 13, 181–194, https://doi.org/10.1007/s11803-014-0222-4, 2014.

https://doi.org/10.5194/egusphere-2025-3248
Preprint. Discussion started: 12 September 2025

Douglas, J.: Ground motion prediction equations 1964–2020, Dept Civ. Env. Eng Univ Strathclyde Glas. UK, 670, 2020.

EPRI: Seismic hazard methodology for the central and eastern United States, Seysmicity Own. Group Electr. Power Res. Inst. EPRI, P101-38-45–46, 2256–14, Report NP-472, 1987.

Epstein, B. and Lomnitz, C.: A Model for the Occurrence of Large Earthquakes, Nature, 211, 954–956, https://doi.org/10.1038/211954b0, 1966.

Ercilla, G., Casas, D., Alonso, B., Casalbore, D., Galindo-Zaldívar, J., García-Gil, S., Martorelli, E., Vázquez, J.-T., Azpiroz-Zabala, M., DoCouto, D., Estrada, F., Fernández-Puga, M. C., González-Castillo, L., González-Vida, J. M., Idárraga-García, J., Juan, C., Macías, J., Madarieta-Txurruka, A., Nespereira, J., Palomino, D., Sánchez-Guillamón, O., Tendero-Salmerón, V., Teixeira, M., Valencia, J., and Yenes, M.: Offshore Geological Hazards: Charting the Course of Progress and Future Directions, Oceans, 2, 393–428, https://doi.org/10.3390/oceans2020023, 2021.

Fernandes, R. M. S., Miranda, J. M., Meijninger, B. M. L., Bos, M. S., Noomen, R., Bastos, L., Ambrosius, B. A. C., and Riva, R. E. M.: Surface velocity field of the Ibero-Maghrebian segment of the Eurasia-Nubia plate boundary, Geophys. J. Int., 169, 315–324, https://doi.org/10.1111/j.1365-246X.2006.03252.x, 2007.

Fonseca, J. F. B. D.: A Reassessment of the Magnitude of the 1755 Lisbon Earthquake, Bull. Seismol. Soc. Am., 110, 1–17, https://doi.org/10.1785/0120190198, 2020.

García Mayordomo, J.: Creación de un modelo de zonas sismogénicas para el cálculo del Mapa de Peligrosidad Sísmica de España, CSIC - Instituto Geológico y Minero de España (IGME), 2015.

García-Fernández, M., Vaccari, F., Jiménez, M.-J., Magrin, A., Romanelli, F., and Panza, G. F.: Chapter 24 - Regional application of the NDSHA approach for continental seismogenic sources in the Iberian Peninsula, in: Earthquakes and Sustainable Infrastructure, edited by: Panza, G. F., Kossobokov, V. G., Laor, E., and De Vivo, B., Elsevier, 491–514, https://doi.org/10.1016/B978-0-12-823503-4.00006-3, 2022.

GEBCO Bathymetric Compilation Group 2024: The GEBCO_2024 Grid - a continuous terrain model of the global oceans and land. NERC EDS British Oceanographic Data Centre NOC., https://doi.org/10.5285/1c44ce99-0a0d-5f4f-e063-7086abc0ea0f, 2024.

Goded, T., Buforn, E., and Muñoz, D.: The 1494 and 1680 Málaga (Southern Spain) Earthquakes, Seismol. Res. Lett., 79, 707–715, https://doi.org/10.1785/gssrl.79.5.707, 2008.

Gonzalez-Castillo, L., Galindo-Zaldivar, J., de Lacy, M. C., Borque, M. J., Martinez-Moreno, F. J., García-Armenteros, J. A., and Gil, A. J.: Active rollback in the Gibraltar Arc: Evidences from CGPS data in the western Betic Cordillera, Tectonophysics, 663, 310–321, https://doi.org/10.1016/j.tecto.2015.03.010, 2015.

Grasso, S. and Maugeri, M.: The Seismic Microzonation of the City of Catania (Italy) for the Etna Scenario Earthquake (M = 6.2) of 20 February 1818, Earthq. Spectra, 28, 573–594, https://doi.org/10.1193/1.4000013, 2012.

Grevemeyer, I., Lange, D., Villinger, H., Custódio, S., and Matias, L.: Seismotectonics of the Horseshoe Abyssal Plain and Gorringe Bank, eastern Atlantic Ocean: Constraints from ocean bottom seismometer data, J. Geophys. Res. Solid Earth, 122, 63–78, https://doi.org/10.1002/2016JB013586, 2017.

Guo, Z., Hong, Y., and Jeng, D.-S.: Structure–Seabed Interactions in Marine Environments, J. Mar. Sci. Eng., 9, 972, https://doi.org/10.3390/jmse9090972, 2021.

https://doi.org/10.5194/egusphere-2025-3248
Preprint. Discussion started: 12 September 2025

Gutscher, M.-A., Malod, J., Rehault, J.-P., Contrucci, I., Klingelhoefer, F., Mendes-Victor, L., and Spakman, W.: Evidence for active subduction beneath Gibraltar, Geology, 30, 1071–1074, https://doi.org/10.1130/0091-7613(2002)030<1071:EFASBG>2.0.CO;2, 2002.

Hamidatou, M., Hallal, N., Lebdioui, S., Agius, M. R., and Sawires, R.: Probabilistic and Deterministic Seismic Hazard Assessments for Northeast Algeria: Insights into the Damaging Impact of the August 7, 2020 (Mw 5.0) Mila Earthquake, Pure Appl. Geophys., https://doi.org/10.1007/s00024-024-03593-y, 2024.

Herraiz, M., De Vicente, G., Lindo-Ñaupari, R., Giner, J., Simón, J. L., González-Casado, J. M., Vadillo, O., Rodríguez-Pascua, M. A., Cicuéndez, J. I., Casas, A., Cabañas, L., Rincón, P., Cortés, A. L., Ramírez, M., and Lucini, M.: The recent (upper Miocene to Quaternary) and present tectonic stress distributions in the Iberian Peninsula, Tectonics, 19, 762–786, https://doi.org/10.1029/2000TC900006, 2000.

Hu, J., Tan, J., and Zhao, J. X.: New GMPEs for the Sagami Bay Region in Japan for Moderate Magnitude Events with Emphasis on Differences on Site Amplifications at the Seafloor and Land Seismic Stations of K-NET, Bull. Seismol. Soc. Am., 110, 2577–2597, https://doi.org/10.1785/0120190305, 2020.

Hu, J., Zhang, W., Hu, L., Ding, L., and Tan, J.: Regional offshore ground motion prediction model from a referenced empirical approach: A case study in the Japan Trench area, Soil Dyn. Earthq. Eng., 174, 108196, https://doi.org/10.1016/j.soildyn.2023.108196, 2023.

Hu, L., Li, Y., and Ji, S.: An offshore non-ergodic ground motion model for subduction earthquakes in Japan Trench area, Earthq. Spectra, 40, 379–419, https://doi.org/10.1177/87552930231207118, 2024.

Idriss, I.: Earthquake Ground Motions at Soft Soil Sites, Int. Conf. Recent Adv. Geotech. Earthq. Eng. Soil Dyn., 1991.

IGN: National Geographic Institute (IGN). Geology and tectonics of Gulf of Cadiz, https://www.ign.es/web/resources/sismologia/tproximos/sismotectonica/pag_sismotectonicas/golfocadiz.html, 2025a.

IGN: National Geographic Institute (IGN). Geology and tectonics of Alboran basin, https://www.ign.es/web/resources/sismologia/tproximos/sismotectonica/pag_sismotectonicas/alboran.html, 2025b.

IGN: National Geographic Institute (IGN). Spanish Seismic Catalogue., https://doi.org/10.7419/162.03.2022, 2025c.

IGN-UPM: Actualización de mapas de peligrosidad sísmica de España 2012, Inst. Geográfico Nac. IGN, 267, https://doi.org/10.7419/162.05.2017, 2017.

Kanazawa, T.: Japan Trench earthquake and tsunami monitoring network of cable-linked 150 ocean bottom observatories and its impact to earth disaster science, in: 2013 IEEE International Underwater Technology Symposium (UT), 2013 IEEE International Underwater Technology Symposium (UT), 1–5, https://doi.org/10.1109/UT.2013.6519911, 2013.

Kanazawa, T., Uehira, K., Mochizuki, M., Shinbo, T., Fujimoto, H., Noguchi, S., Kunugi, T., Shiomi, K., Aoi, S., and Matsumoto, T.: S-net project, cabled observation network for earthquakes and tsunamis, Abstract WE2B–3 presented at SubOptic 2016, Suboptic, Dubai, 18–21 April, 2016.

Kariche, J., Meghraoui, M., Timoulali, Y., Cetin, E., and Toussaint, R.: The Al Hoceima earthquake sequence of 1994, 2004 and 2016: Stress transfer and poroelasticity in the Rif and Alboran Sea region, Geophys. J. Int., 212, 42–53, https://doi.org/10.1093/gji/ggx385, 2018.

https://doi.org/10.5194/egusphere-2025-3248
Preprint. Discussion started: 12 September 2025

Karthigeyan, V.: A review of current practice and future trends in the design of offshore installations to withstand seismic hazard, in: Seismic Design and Practice into the Next Century, Routledge, London, 2022.

Kee, T. K., Cheok, C. J., Kamarudin, M. A., Ahmad, S. W., and Suryanti, R.: Seismic Effect of the Offshore Structure Under Different Earthquake Loadings, Int. J. Integr. Eng., 15, 256–262, https://doi.org/10.30880/ijie.2023.15.02.025, 2023.

Khellafi, A. M., Harichane, Z., Afra, H., and Sadouki, A.: A Case Study of Accelerometric Records Analysis of May 21st, 2003, Boumerdes (Algeria) Earthquake, Int. J. Geotech. Earthq. Eng. IJGEE, 4, 34–52, https://doi.org/10.4018/ijgee.2013070103, 2013.

Kijko, A.: Seismic Hazard, in: Encyclopedia of Solid Earth Geophysics, edited by: Gupta, H. K., Springer International Publishing, Cham, 1–14, https://doi.org/10.1007/978-3-030-10475-7_10-1, 2019.

Kiureghian, A. D. and Ditlevsen, O.: Aleatory or epistemic? Does it matter?, Struct. Saf., 31, 105–112, https://doi.org/10.1016/j.strusafe.2008.06.020, 2009.

Kossobokov, V. and Panza, G.: Seismic roulette: Hazards and risks, Terra Nova, 34, 475–494, https://doi.org/10.1111/ter.12617, 2022.

Kotha, S. R., Weatherill, G., Bindi, D., and Cotton, F.: A regionally-adaptable ground-motion model for shallow crustal earthquakes in Europe, Bull. Earthq. Eng., 18, 4091–4125, https://doi.org/10.1007/s10518-020-00869-1, 2020.

Kramer, S. L.: Geotechnical Earthquake Engineering, Prentice-Hall Civ. Eng. Eng. Mech. Ser. Prentice Hall Up. Saddle River, 653, 1996.

Krinitzsky, E. L.: Deterministic versus probabilistic seismic hazard analysis for critical structures, Eng. Geol., 40, 1–7, https://doi.org/10.1016/0013-7952(95)00031-3, 1995.

Krinitzsky, E. L.: How to obtain earthquake ground motions for engineering design, Eng. Geol., 65, 1–16, https://doi.org/10.1016/S0013-7952(01)00098-9, 2002.

Kumar, V., Khan, P. K., Sarkar, R., and Pal, S. K.: Seismic hazard assessment of Faizabad region of Uttar Pradesh, India, utilizing deterministic and probabilistic approaches, J. Earth Syst. Sci., 134, 8, https://doi.org/10.1007/s12040-024-02451-8, 2024.

Lafuerza, S., Sultan, N., Canals, M., Lastras, G., Cattaneo, A., Frigola, J., Costa, S., and Berndt, C.: Failure mechanisms of Ana Slide from geotechnical evidence, Eivissa Channel, Western Mediterranean Sea, Mar. Geol., 307–310, 1–21, https://doi.org/10.1016/j.margeo.2012.02.010, 2012.

Lan, J., Liu, J., and Song, X.: Study on the influence of the seafloor soft soil layer on seismic ground motion, Nat. Hazards Earth Syst. Sci., 21, 577–585, https://doi.org/10.5194/nhess-21-577-2021, 2021.

Leprêtre, R., Frizon de Lamotte, D., Combier, V., Gimeno-Vives, O., Mohn, G., and Eschard, R.: The Tell-Rif orogenic system (Morocco, Algeria, Tunisia) and the structural heritage of the southern Tethys margin, BSGF-Earth Sci. Bull., 189, 10, https://doi.org/10.1051/bsgf/2018009, 2018.

Li, C., Diao, Y.-C., Li, R.-H., Pan, H.-Y., Han, Q., and Li, H.-N.: Effect of soil spatial variability on characteristics of depth-varying multi-support seismic motions at offshore sites, Soil Dyn. Earthq. Eng., 174, 108195, https://doi.org/10.1016/j.soildyn.2023.108195, 2023.

https://doi.org/10.5194/egusphere-2025-3248
Preprint. Discussion started: 12 September 2025

Liu, H., Yang, Y., and Peng, J.: A Unified Model for Analyzing Comprehensive Behaviors of Deepwater Anchors, J. Mar. Sci. Eng., 9, 913, https://doi.org/10.3390/jmse9080913, 2021.

López Arroyo, A. and Udías, A.: Aftershock sequence and focal parameters of the February 28, 1969 earthquake of the Azores-Gibraltar fracture zone, Bull. Seismol. Soc. Am., 62, 699–719, https://doi.org/10.1785/BSSA0620030699, 1972.

Martín Míguez, B., Novellino, A., Vinci, M., Claus, S., Calewaert, J.-B., Vallius, H., Schmitt, T., Pititto, A., Giorgetti, A., Askew, N., Iona, S., Schaap, D., Pinardi, N., Harpham, Q., Kater, B. J., Populus, J., She, J., Palazov, A. V., McMeel, O., Oset, P., Lear, D., Manzella, G. M. R., Gorringe, P., Simoncelli, S., Larkin, K., Holdsworth, N., Arvanitidis, C. D., Molina Jack, M. E., Chaves Montero, M. del M., Herman, P. M. J., and Hernandez, F.: The European Marine Observation and Data Network (EMODnet): Visions and Roles of the Gateway to Marine Data in Europe, Front. Mar. Sci., 6, https://doi.org/10.3389/fmars.2019.00313, 2019.

Martín-Dávila, J. and Pazos, A.: Sismicidad del Golfo de Cadiz y zonas adyacentes, Física Tierra ISSN 0214-4557 Nº 15 2003 Pags 189-210, 2003.

Martínez-Loriente, S., Gràcia, E., Bartolome, R., Sallarès, V., Connors, C., Perea, H., Lo Iacono, C., Klaeschen, D., Terrinha, P., Dañobeitia, J. J., and Zitellini, N.: Active deformation in old oceanic lithosphere and significance for earthquake hazard: Seismic imaging of the Coral Patch Ridge area and neighboring abyssal plains (SW Iberian Margin), Geochem. Geophys. Geosystems, 14, 2206–2231, https://doi.org/10.1002/ggge.20173, 2013.

Mayer, L., Jakobsson, M., Allen, G., Dorschel, B., Falconer, R., Ferrini, V., Lamarche, G., Snaith, H., and Weatherall, P.: The Nippon Foundation—GEBCO Seabed 2030 Project: The Quest to See the World's Oceans Completely Mapped by 2030, Geosciences, 8, 63, https://doi.org/10.3390/geosciences8020063, 2018.

McGuire, R. K.: FORTRAN computer program for seismic risk analysis, US Geological Survey, 1976.

McGuire, R. K.: Seismic hazard and risk analysis, Earthquake Engineering Research Institute, Berkeley, 2004.

McGuire, R. K.: Probabilistic seismic hazard analysis: Early history, Earthq. Eng. Struct. Dyn., 37, 329–338, https://doi.org/10.1002/eqe.765, 2008.

McGuire, R. K. and Shedlock, K. M.: Statistical uncertainties in seismic hazard evaluations in the United States, Bull. Seismol. Soc. Am., 71, 1287–1308, https://doi.org/10.1785/BSSA0710041287, 1981.

Mendes-Victor, L. A., Oliveira, C. S., Azevedo, J., and Ribeiro, A.: The 1755 Lisbon Earthquake: Revisited, Springer Netherlands, Dordrecht, https://doi.org/10.1007/978-1-4020-8609-0, 2009.

Molina Palacios, S.: Sismotectónica y peligrosidad sísmica del área de contacto entre Iberia y África, http://purl.org/dc/dcmitype/Text, Universidad de Granada, 1998.

Morikawa, N. and Fujiwara, H.: A New Ground Motion Prediction Equation for Japan Applicable up to M9 Mega-Earthquake, J. Disaster Res., 8, 878–888, https://doi.org/10.20965/jdr.2013.p0878, 2013.

Mostafa, S. I., Abdelhafiez, H. E., and Abd el-aal, A. el-aziz K.: Deterministic scenarios for seismic hazard assessment in Egypt, J. Afr. Earth Sci., 160, 103655, https://doi.org/10.1016/j.jafrearsci.2019.103655, 2019.

Mourabit, T., Abou Elenean, K. M., Ayadi, A., Benouar, D., Ben Suleman, A., Bezzeghoud, M., Cheddadi, A., Chourak, M., ElGabry, M. N., Harbi, A., Hfaiedh, M., Hussein, H. M., Kacem, J., Ksentini, A., Jabour, N., Magrin, A., Maouche, S.,

https://doi.org/10.5194/egusphere-2025-3248
Preprint. Discussion started: 12 September 2025

Meghraoui, M., Ousadou, F., Panza, G. F., Peresan, A., Romdhane, N., Vaccari, F., and Zuccolo, E.: Neo-deterministic seismic hazard assessment in North Africa, J. Seismol., 18, 301–318, https://doi.org/10.1007/s10950-013-9375-2, 2014.

Musson, R. M. W.: Probability in PSHA: Reply to "Comment on 'PSHA Validated by Quasi-Observational Means' by Z. Wang," Seismol. Res. Lett., 83, 717–719, https://doi.org/10.1785/0220120036, 2012a.

Musson, R. M. W.: PSHA Validated by Quasi Observational Means, Seismol. Res. Lett., 83, 130–134, https://doi.org/10.1785/gssrl.83.1.130, 2012b.

Nakanishi, R. and Takemura, S.: Development of an offshore ground motion prediction equation for peak ground acceleration considering path effects based on S-net data, Earth Planets Space, 76, 146, https://doi.org/10.1186/s40623-024-02078-5, 2024.

Neres, M., Carafa, M. M. C., Fernandes, R. M. S., Matias, L., Duarte, J. C., Barba, S., and Terrinha, P.: Lithospheric deformation in the Africa-Iberia plate boundary: Improved neotectonic modeling testing a basal-driven Alboran plate, J. Geophys. Res. Solid Earth, 121, 6566–6596, https://doi.org/10.1002/2016JB013012, 2016.

Nishikawa, T., Ide, S., and Nishimura, T.: A review on slow earthquakes in the Japan Trench, Prog. Earth Planet. Sci., 10, 1, https://doi.org/10.1186/s40645-022-00528-w, 2023.

Nocquet, J.-M.: Present-day kinematics of the Mediterranean: A comprehensive overview of GPS results, Tectonophysics, 579, 220–242, https://doi.org/10.1016/j.tecto.2012.03.037, 2012.

NRC: Reactor site criteria. Appendix a: seismic and geology siting criteria for nuclear power plants, US Nucl. Regul. Comm. NRC Regul. Guide 10CFR100, 1973.

Orozova, I. M. and Suhadolc, P.: A deterministic–probabilistic approach for seismic hazard assessment, Tectonophysics, 312, 191–202, https://doi.org/10.1016/S0040-1951(99)00162-6, 1999.

Pagani, M., Monelli, D., Weatherill, G., Danciu, L., Crowley, H., Silva, V., Henshaw, P., Butler, L., Nastasi, M., Panzeri, L., Simionato, M., and Vigano, D.: OpenQuake Engine: An Open Hazard (and Risk) Software for the Global Earthquake Model, Seismol. Res. Lett., 85, 692–702, https://doi.org/10.1785/0220130087, 2014.

Palano, M., González, P. J., and Fernández, J.: Strain and stress fields along the Gibraltar Orogenic Arc: Constraints on active geodynamics, Gondwana Res., 23, 1071–1088, https://doi.org/10.1016/j.gr.2012.05.021, 2013.

Panza, G. F., Prozorov, A. G., and Suhadolc, P.: Lithosphere structure and statistical properties of seismicity in Italy and surrounding regions, J. Geodyn., 12, 189–215, https://doi.org/10.1016/0264-3707(90)90007-H, 1990.

Peresan, A., Magrin, A., Nekrasova, A., Kossobokov, V. G., and Panza, G. F.: Earthquake recurrence and seismic hazard assessment: a comparative analysis over the Italian territory, in: Proceedings of the ERES 2013 Conference. WIT transactions on the built environment, 23–34, https://doi.org/10.2495/ERES130031, 2013.

Poggi, V., Garcia-Peláez, J., Styron, R., Pagani, M., and Gee, R.: A probabilistic seismic hazard model for North Africa, Bull. Earthq. Eng., 18, 2917–2951, https://doi.org/10.1007/s10518-020-00820-4, 2020.

Randolph, M. and Gourvenec, S.: Offshore Geotechnical Engineering, CRC Press, London, 560 pp., https://doi.org/10.1201/9781315272474, 2017.

https://doi.org/10.5194/egusphere-2025-3248
Preprint. Discussion started: 12 September 2025

Reilly, W. I., Fredrich, G., Hein, G. W., Landau, H., Almazán, J. L., and Caturla, J. L.: Geodetic determination of crustal deformation across the Strait of Gibraltar, Geophys. J. Int., 111, 391–398, https://doi.org/10.1111/j.1365-246X.1992.tb00585.x, 1992.

Reiter, L.: Earthquake Hazard Analysis: Issues and Insights, Columbia University Press, 254 pp., 1990.

Ritsema, J., Lay, T., and Kanamori, H.: The 2011 Tohoku Earthquake, Elements, 8, 183–188, https://doi.org/10.2113/gselements.8.3.183, 2012.

Rodriguez, M., Maleuvre, C., Jollivet-Castelot, M., d'Acremont, E., Rabaute, A., Lafosse, M., Ercilla, G., Vázquez, J.-T., Alonso, B., Ammar, A., and Gorini, C.: Tsunamigenic submarine landslides along the Xauen–Tofiño banks in the Alboran Sea (Western Mediterranean Sea), Geophys. J. Int., 209, 266–281, https://doi.org/10.1093/gji/ggx028, 2017.

Román-de la Sancha, A., Silva, R., Areu-Rangel, O. S., Verduzco-Zapata, M. G., Mendoza, E., López-Acosta, N. P., Ossa, A., and García, S.: Modelling the sequential earthquake–tsunami response of coastal road embankment infrastructure, Nat. Hazards Earth Syst. Sci., 22, 2589–2609, https://doi.org/10.5194/nhess-22-2589-2022, 2022.

Rui, S., Zhang, H., Xu, H., Zha, X., Xu, M., and Shen, K.: Seabed structures and foundations related to deep-sea resource development: A review based on design and research, Deep Undergr. Sci. Eng., 3, 131–148, https://doi.org/10.1002/dug2.12042, 2024.

Sá, L. F., Morales-Esteban, A., and Neyra, P. D.: A deterministic seismic risk macrozonation of Seville, Arab. J. Geosci., 14, 2392, https://doi.org/10.1007/s12517-021-08626-7, 2021.

Salgado Gálvez, M. A., Cardona Arboleda, O. D., Carreño Tibaduiza, M. L., and Barbat Barbat, H. A.: Probabilistic seismic hazard and risk assessment in Spain: national and local level case studies, Centre Internacional de Mètodes Numèrics en Enginyeria (CIMNE), 2015.

Shan, Z., Wu, H., Ni, W., Sun, M., Wang, K., Zhao, L., Lou, Y., Liu, A., Xie, W., Zheng, X., and Guo, X.: Recent Technological and Methodological Advances for the Investigation of Submarine Landslides, J. Mar. Sci. Eng., 10, 1728, https://doi.org/10.3390/jmse10111728, 2022.

Silva, P. G., Elez, J., Giner-Robles, J., Perez-Lopez, R., Roquero, E., Rodriguez-Pascua, M., Azcárate, T., and Martínez-Graña, A.: ANÁLISIS GEOLÓGICO DEL TERREMOTO DE TORREVIEJA DE 1829 (ALICANTE, SE ESPAÑA), 2019.

Silva, V., Crowley, H., Pagani, M., Monelli, D., and Pinho, R.: Development of the OpenQuake engine, the Global Earthquake Model's open-source software for seismic risk assessment, Nat. Hazards, 72, 1409–1427, https://doi.org/10.1007/s11069-013-0618-x, 2014.

Stich, D., Batlló, J., Morales, J., Macià, R., and Dineva, S.: Source parameters of the MW= 6.1 1910 Adra earthquake (southern Spain), Geophys. J. Int., 155, 539–546, https://doi.org/10.1046/j.1365-246X.2003.02059.x, 2003.

Sultan, N., Gaudin, M., Berne, S., Canals, M., Urgeles, R., and Lafuerza, S.: Analysis of slope failures in submarine canyon heads: An example from the Gulf of Lions, J. Geophys. Res. Earth Surf., 112, https://doi.org/10.1029/2005JF000408, 2007.

Tan, J. and Hu, J.: Offshore ground motion characteristics on the horizontal PGA, spectral acceleration, frequency content and significant duration from the 2021 Mw 7.1 and 2022 Mw 7.4 offshore earthquakes near the Japan Trench area, Soil Dyn. Earthq. Eng., 164, 107646, https://doi.org/10.1016/j.soildyn.2022.107646, 2023.

https://doi.org/10.5194/egusphere-2025-3248
Preprint. Discussion started: 12 September 2025

Udias, A. and Muñoz, D.: The Andalusian earthquake of 25 December 1884, Tectonophysics, 53, 291–299, https://doi.org/10.1016/0040-1951(79)90074-X, 1979.

Vázquez, J.-T., Ercilla, G., Alonso, B., Peláez, J. A., Palomino, D., León, R., Bárcenas, P., Casas, D., Estrada, F., Fernández-Puga, M. C., Galindo-Zaldívar, J., Henares, J., Llorente, M., Sánchez-Guillamón, O., d'Acremont, E., Ammar, A., Chourak, M., Fernández-Salas, L. M., López-González, N., and Lafuerza, S.: Triggering Mechanisms of Tsunamis in the Gulf of Cadiz and the Alboran Sea: An Overview, in: Historical Earthquakes, Tsunamis and Archaeology in the Iberian Peninsula, edited by: Álvarez-Martí-Aguilar, M. and Machuca Prieto, F., Springer Nature, Singapore, 65–104, https://doi.org/10.1007/978-981-19-1979-4_4, 2022.

Veiskarami, M., Neshaei, M. A. L., Karimpour Fard, M., and Pourramezan, T.: Numerical study on static and seismic stability of breakwaters on soft granular marine deposits against deep failure, Mar. Georesources Geotechnol., 35, 42–51, https://doi.org/10.1080/1064119X.2015.1099063, 2017.

Wang, B., Hu, S., Song, G., and Chen, B.: The Influences of the Offshore Ground Motion and Site Factors on the Seismic Response of Immersed Tunnels, Int. J. Struct. Stab. Dyn., 24, 2450276, https://doi.org/10.1142/S0219455424502766, 2024.

Wang, J.-P., Huang, D., and Yang, Z.: Deterministic seismic hazard map for Taiwan developed using an in-house Excel-based program, Comput. Geosci., 48, 111–116, https://doi.org/10.1016/j.cageo.2012.05.014, 2012.

Wang, Z.: Seismic Hazard Assessment: Issues and Alternatives, Pure Appl. Geophys., 168, 11–25, https://doi.org/10.1007/s00024-010-0148-3, 2011.

Wang, Z.: Comment on "PSHA Validated by Quasi Observational Means" by R. M. W. Musson, Seismol. Res. Lett., 83, 714–716, https://doi.org/10.1785/0220120016, 2012.

Wang, Z. and Cobb, J. C.: A critique of probabilistic versus deterministic seismic hazard analysis with special reference to the New Madrid seismic zone, Recent Adv. North Am. Paleoseismology Neotectonics East Rock., 2012.

Weatherill, G. and Cotton, F.: A ground motion logic tree for seismic hazard analysis in the stable cratonic region of Europe: regionalisation, model selection and development of a scaled backbone approach, Bull. Earthq. Eng., 18, 6119–6148, https://doi.org/10.1007/s10518-020-00940-x, 2020.

Wössner, J., Laurentiu, D., Giardini, D., Crowley, H., Cotton, F., Grünthal, G., Valensise, G., Arvidsson, R., Basili, R., Demircioglu, M. B., Hiemer, S., Meletti, C., Musson, R. W., Rovida, A. N., Sesetyan, K., Stucchi, M., and The SHARE Consortium: The 2013 European Seismic Hazard Model: key components and results, Bull. Earthq. Eng., 13, 3553–3596, https://doi.org/10.1007/s10518-015-9795-1, 2015.

Zhao, J. X., Zhang, J., Asano, A., Ohno, Y., Oouchi, T., Takahashi, T., Ogawa, H., Irikura, K., Thio, H. K., Somerville, P. G., Fukushima, Y., and Fukushima, Y.: Attenuation Relations of Strong Ground Motion in Japan Using Site Classification Based on Predominant Period, Bull. Seismol. Soc. Am., 96, 898–913, https://doi.org/10.1785/0120050122, 2006.